

Thermal analysis for non-Newtonian fluids flow over a curved stretchable surface with carbon nanotubes suspension



by

Zain Ul Abideen

(Registration No: 00000360423)

A thesis submitted in partial fulfilment of the requirements for the degree of
Master of Science in Mathematics

Supervised by:


Dr. Rai Sajjad Saif

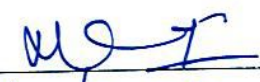
Department of Mathematics, School of Natural Sciences, National University of
Sciences and Technology, Islamabad, Pakistan


©Zain Ul Abideen, 2023

THESIS ACCEPTANCE CERTIFICATE

Certified that final copy of MS thesis written by Zain ul Abideen (Registration No. 00000360423), of School of Natural Sciences has been vetted by undersigned, found complete in all respects as per NUST statutes/regulations, is free of plagiarism, errors, and mistakes and is accepted as partial fulfillment for award of MS/M.Phil degree. It is further certified that necessary amendments as pointed out by GEC members and external examiner of the scholar have also been incorporated in the said thesis.

Signature:  31-08-23
Name of Supervisor: Dr. Rai Sajjad Saif
Date: _____

Signature (HoD): 
Date: 31/08/2023

Signature (Dean/Principal): 
Date: 04.09.2023

National University of Sciences & Technology**MS THESIS WORK**

We hereby recommend that the dissertation prepared under our supervision by: "Zain ul Abideen" Regn No. 00000360423 Titled: "Thermal Analysis for Non-Newtonian Fluid Flows Over a Curved Stretchable Surface with Carbon Nanotubes Suspension" accepted in partial fulfillment of the requirements for the award of **MS** degree.

Examination Committee Members1. Name: Prof. Meraj Mustafa HashmiSignature: 2. Name: Dr. Muhammad Asif FarooqSignature: Supervisor's Name: Dr. Rai Sajjad SaifSignature: 


Head of Department

31/08/2023
Date

COUNTERSIGNEDDate: 09.09.2023


Dean/Principal

Dedication

This thesis is dedicated to my beloved parents and siblings for their continuous support and motivation.

Acknowledgment

First and foremost, I am greatly thankful to my **ALLAH Almighty** the most Generous and Merciful. **ALHUMDULILLAH.**

It was an honour for me to work under the supervision of **Dr. Rai Sajjad Saif**. Words will not do justice to extend my heartfelt appreciations for him. During my research period, he kept me well motivated and well directed. I want to thank him for his continuous support, motivation and patience. **JazakALLAH o Khair.**

I would also like to extend my warmest thanks to my respected GEC members, **Dr. Meraj Mustafa Hashmi** and **Dr. Muhammad Asif Farooq**, for their co-operation, insight comments and interesting questions.

This acknowledgement will be of no worth unless I extend my heartfelt appreciations to my beloved parents **Mr. Muhammad Afzal, Ms. Naseem Afzal** and siblings **Mr. Mohammad Waleed Afzal** and **Ms. Rabia Basri** for their love, sacrifices, motivations and continuous support in every regard.

There is a huge list of people who made my journey at NUST full of beautiful memories. They are my second family at my second home NUST. Unfortunately I can't list them all here. I would like to extend my deep-felt thanks to a friend **Ms. Ramsha Arshad** who is more like a blessing I am blessed with at NUST. Thanks for always being there and motivating me in every regard throughout my journey at NUST and after, **Gracias Dost!** I would also like to say thanks to all my fellows at NUST, **Zoya Jamil, Misbah Humayun, Muhammad Haseeb Zafar, Abdullah Zahid Khan, Mohammad Danish** and **Ammar Adnan** to name a few. Thanks to these souls for always uplifting me, comforting me, believing in me and supporting me. I will be very grateful to you guys for the rest of my life.

Zain Ul Abideen

Abstract

In this thesis heat transmission of non-Newtonian radiative nanofluids flow is inspected with reference to boundary layer description. Carbon nanotubes (CNTs) dependent fluids are being evaluated by considering the geometry of curved stretchable surface. Special features, like thermal radiation and internal heat generation, which corresponds to heat transmission along the flow have been incorporated. Dual nature of carbon nanotubes, that is, single walled carbon nanotubes (SWCNTs) as well as multiple walled carbon nanotubes (MWCNTs) together with blood and slurry mixture (base fluids) have been utilized for the composition of nanofluid. In order to capture the rheological properties of blood, Casson fluid model has been deployed. Likewise, second-grade model has been engaged to capture the rheological properties of slurry mixture. Appropriate similarity transformations have been applied to reduce the modelled system of nonlinear partial differential equations into a system of ordinary differential equations (ODEs). To achieve the desired numerical solution of obtained system of ODEs, NDSolve technique is employed using Mathematica. Numerous parameters appearing in governing equations, exert influence on focused physical quantities. Graphs have been engaged to capture these variations for both SWCNTs and MWCNTs. Likewise, numeric charts have been displayed to investigate impressions on skin friction coefficient and Nusselt number for distinct parameters.

List of Figures

Fig. 1. 1: Illustrative diagram of laminar and turbulent flows	2
Fig. 1. 1: Illustrative diagram of boundary layer formation	9
Fig. 2. 1: Geometrical view of the problem	18
Fig. 2. 2: Action of (κ) on $f'(\zeta)$	25
Fig. 2. 3: Action of (φ) on $f'(\zeta)$	25
Fig. 2. 4: Action of (β^c) on $f'(\zeta)$	26
Fig. 2. 5: Action of (κ) on $\theta(\zeta)$	26
Fig. 2. 6: Action of (λ_l) on $\theta(\zeta)$	26
Fig. 2. 7: Action of (φ) on $\theta(\zeta)$	26
Fig. 2. 8: Action of (R_D) on $\theta(\zeta)$	27
Fig. 2. 9: Action of (κ) on $P(\zeta)$	27
Fig. 2.10: Action of (κ) on $P'(\zeta)$	27
Fig. 2. 11: Action of (κ) on (C_f)	28
Fig. 2. 12: Action of (κ) on (Nu)	28
Fig. 3. 1: Action of (κ) over $f'(\zeta)$	41
Fig. 3. 2: Action of (φ) over $f'(\zeta)$	41
Fig. 3. 3: Action of (α_l) over $f'(\zeta)$	42
Fig. 3. 4: Action of (κ) over $\theta(\zeta)$	42
Fig. 3. 5: Action of (φ) over $\theta(\zeta)$	42
Fig. 3. 6: Action of (λ_l) over $\theta(\zeta)$	42
Fig. 3. 7: Action of (R_D) over $\theta(\zeta)$	43
Fig. 3. 8: Action of (κ) over $P(\zeta)$	43
Fig. 3. 9: Action of (κ) over $P'(\zeta)$	43
Fig. 3.10: Action of (κ) over (C_f)	44
Fig. 3. 11: Action of (κ) over (Nu)	44

List of Tables

Table 2. 1: Thermophysical characteristics of Casson fluid and carbon nanotubes (SWCNTs and MWCNTs).....	21
Table 2. 2: Numerical data for local Nusselt number and skin friction coefficient for various parameters.	29
Table 2. 3: Error analysis of the values of $-Re_{sd}^{1/2} C_f$ to address the validity of numerical method with $R_D = \beta^c = \lambda_l = 0$	29
Table 2. 4: Comparative analysis of the values of $-Re_{sd}^{1/2} C_f$ for distinct numerics of κ and φ with $R_D = \lambda_l = 0$ and $\beta^c \rightarrow 0$	30
Table 3. 1: Thermophysical characteristics of carbon nanotubes (SWCNTs and MWCNTs) 37	
Table 3. 2: Numerical data for local Nusselt number and skin friction coefficient for various parameters	45
Table 3. 3: Error analysis of the values of $-Re_{sd}^{1/2} C_f$ to address the validity of numerical method with $R_D = \lambda_l = \alpha_l = 0$	46
Table 3. 4: Comparative analysis of the values of $-Re_{sd}^{1/2} C_f$ for distinct numerics of κ and φ , with $R_D = \lambda_l = \alpha_l = 0$	46

Contents

1	Introduction	1
1.1	Basic definitions and preliminaries	1
1.1.1	Compressible and incompressible flows	1
1.1.2	Steady and unsteady flows	1
1.1.3	Laminar and turbulent flows	2
1.1.4	Newtonian fluids	3
1.1.5	Non-Newtonian fluids	3
1.2	Conservation laws	4
1.2.1	Conservation law of mass	5
1.2.2	Conservation law of momentum	5
1.2.3	Conservation law of energy	5
1.3	Nanofluids	6
1.3.1	Tiwari and Das model	6
1.3.2	Buongiorno Model	7
1.4	Boundary layer flow	8
1.5	Some dimensionless numbers	9
1.5.1	Reynolds number	9
1.5.2	Prandtl number	9
1.5.3	Nusselt number	10
1.6	Heat transfer	10
1.6.1	Conduction	10
1.6.2	Convection	11

1.6.3	Radiation	11
1.7	Methodology	11
1.7.1	Shooting technique	11
1.8	Literature review	12
1.9	Research objectives	15
2	Impact of thermal radiation and internal heat generation on Casson nanofluid flowing by a curved stretchable surface with suspension of carbon nanotubes	17
2.1	Mathematical analysis	18
2.2	Numerical solution and discussion	22
2.3	Conclusions	30
3	Second-grade fluid with carbon nanotubes flowing over a curved stretchable surface possessing thermal radiation and internal heat generation effects	32
3.1	Mathematical analysis	32
3.2	Numerical solution and discussion	37
3.3	Conclusions	46
	Bibliography	48

Chapter 1

Introduction

This chapter educates some basic definitions and preliminaries. A description for boundary layer flow and some affiliated dimensionless numbers utilized in this thesis are elaborated. Mathematical models, showcasing the interdependence of physical properties of nanofluids are also included. Further, a deep literature review is presented along with a brief description about the numerical technique employed.

1.1 Basic definitions and preliminaries

1.1.1 Compressible and incompressible flows

Incompressible flows refer to the fluid flows where the fluid exhibits unvarying density across the entire flow field. Majority of the liquids are typically regarded as incompressible fluids. However, fluid flows where the density owns a change either in relation to time or spatial coordinates are referred to as compressible fluid flows. The flow of gases is commonly considered as compressible.

1.1.2 Steady and unsteady flows

The fluid flows during which all the physical characteristics (i.e. density, velocity, temperature etc.) stay invariant over time (i.e. flow is independent of time) but may vary from point to

point are regarded as steady fluid flows. Mathematically, for any quantity Ψ :

$$\frac{\partial \Psi}{\partial t} = 0, \quad (1.1)$$

For unsteady fluid flows, at least one physical quantity is time dependent

$$\frac{\partial \Psi}{\partial t} \neq 0, \quad (1.2)$$

for some physical quantity Ψ .

1.1.3 Laminar and turbulent flows

Laminar flows are identified as flows in which fluid particles moves in parallel layers and stream lines do not intersect each other. In contrast, turbulent flows are elucidated with irregular and chaotic motion, with fluid particles swirling and mixing in unpredictable patterns i.e. fluid particles do not follow specific paths. Pouring honey from a jar can be described as laminar flow as it flows in a smooth and steady stream. While the flow of water in waterfalls where water particles rush and fall in a disorderly manner can be signified as turbulent flow.

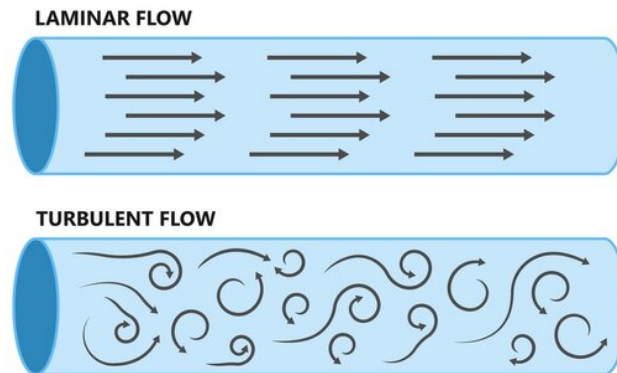


Fig. (1.1) Illustrative diagram of laminar and turbulent flows

1.1.4 Newtonian fluids

These fluids are in agreement with Newton's law of viscosity, expressed below:

$$\tau_{yx} = \mu \frac{dx_s}{dy}, \quad (1.3)$$

where τ_{yx} indicates shear stress in x -direction, μ describes fluid's dynamic viscosity and $\frac{dx_s}{dy}$ expresses deformation rate for one-dimensional and uni-directional flow overtop a plane surface. Eq. (1.3), elucidates that shear stress is directly proportional to deformation rate. Water and air are some conventional Newtonian fluids.

1.1.5 Non-Newtonian fluids

Non-Newtonian fluids are categorized as fluids possessing nonlinear relationship between shear rate and shear stress. Consequently, viscosity of non-Newtonian fluids varies with deformation rate. Power law model illustrates the relation between shear rate and shear stress as follows:

$$\tau_{yx} = \gamma \left(\frac{dx_s}{dy} \right)^n, \quad (1.4)$$

where flow behavior index is expressed as n and γ signifies consistency index. Power law model can also be expressed as:

$$\tau_{yx} = \hat{\gamma} \frac{dx_s}{dy}, \quad (1.5)$$

where, $\hat{\gamma} = \gamma \left(\frac{dx_s}{dy} \right)^{n-1}$ elucidates apparent viscosity of the fluid.

The study of non-Newtonian fluids has acquired significant engagement in the field of fluid dynamics owing to their unparalleled behavior and wide-reaching applications. These fluids have insightful importance in wide-ranging industrial units, encompassing cosmetics, food processing, pharmaceuticals and oil drilling. Interpreting the rheological features and flow manner of non-Newtonian fluids is vital for enhancing processes, upgrading product quality and guaranteeing optimal operations. Real-life applications of non-Newtonian fluids incorporate gels, paints, slurry mixtures and even bodily fluids like mucus and blood. Many scientists proposed various models to capture the rheological properties of different non-Newtonian fluids. Some famous models are given below:

Casson fluid

Another useful model possessing diverse industrial applications is Casson fluid model. Following equation elucidates the rheological characteristics of Casson fluid.

$$\boldsymbol{\tau}_{jk} = \begin{cases} 2 (\mu_p + p_s/\sqrt{2\pi}) a_{jk} & \text{if } \pi > \pi_c, \\ 2 (\mu_p + p_s/\sqrt{2\pi_c}) a_{jk} & \text{if } \pi < \pi_c, \end{cases} \quad (1.6)$$

where a_{jk} stands for $(j, k)^{th}$ component of deformation rate and π is the self product of deformation rate component. Based on non-Newtonian model π_c indicates critical value of product and μ_p and p_s portray plastic dynamic viscosity and yield stress of the fluid respectively.

Second-grade fluid

One of many proposed non-Newtonian liquids is second-grade fluid, which possesses stress tensor relationship with dual derivatives. The second-grade fluid possess an extra stress tensor [24] defined as

$$\boldsymbol{\tau} = -p\mathbf{I} + \mu\mathbf{A}_1 + \alpha_1\mathbf{A}_2 + \alpha_2\mathbf{A}_1^2, \quad (1.7)$$

where p denotes pressure, \mathbf{I} indicates identity tensor, μ is dynamic viscosity, α_j ($j = 1, 2$) are second grade material constants and the first two Rivlin-Ericksen tensors \mathbf{A}_1 and \mathbf{A}_2 are described as

$$\left. \begin{aligned} \mathbf{A}_1 &= (\text{grad } \mathbf{V})^t + (\text{grad } \mathbf{V}), \\ \mathbf{A}_2 &= \mathbf{A}_1(\text{grad } \mathbf{V}) + \frac{d\mathbf{A}_1}{dt} + (\text{grad } \mathbf{V})^t \mathbf{A}_1, \end{aligned} \right\} \quad (1.8)$$

in which d/dt is material time derivative and \mathbf{V} is the velocity vector. This fact should be noticed that when $\alpha_1 = \alpha_2 = 0$, the fundamental equation for second grade fluid reduces to that of viscous fluid. Some common examples of second-grade fluid are latex paints and cornstarch. Some common examples of casson fluid are honey, jelly and tomato sauce.

1.2 Conservation laws

The governing nonlinear differential equations for any flow field are based of conservations laws of mechanics. The laws of conservation of mass, momentum and energy are documented as

follows:

1.2.1 Conservation law of mass

Conservation law of mass can be declared as: the amount of mass of fluid entering and evacuating the (small fixed) control volume stays the same over time i.e. $\dot{m}_{out} - \dot{m}_{in} = 0$. Where \dot{m}_{in} and \dot{m}_{out} indicate mass of fluid entering and evacuating the control volume per unit time respectively. Mathematically, conservation law of mass can be written as:

$$\frac{\partial \rho}{\partial t} + \vec{\nabla} \cdot (\rho \mathbf{V}) = 0, \quad (1.9)$$

where ρ signifies fluid's density, $\vec{\nabla}$ defines gradient operator and \mathbf{V} stands for velocity vector. If the density of fluid is know, then velocity of fluid can simply be determined. For steady and incompressible fluid Eq. (1.9) yields:

$$\vec{\nabla} \cdot \mathbf{V} = 0. \quad (1.10)$$

1.2.2 Conservation law of momentum

Conservation law of mass specifies that, the sum of all (body and surface) forces acting upon a unit volume of fluid is equal to the time rate of change of linear momentum of a moving unit volume of fluid. Conservation law of momentum possesses following vector form:

$$\rho \frac{d\mathbf{V}}{dt} = -\vec{\nabla} p + \vec{\nabla} \cdot \boldsymbol{\tau} + \rho \vec{F}, \quad (1.11)$$

where d/dt stands for material derivative, p defines pressure, $\vec{\nabla} \cdot \boldsymbol{\tau}$ depicts the divergence of stress tensor $\boldsymbol{\tau}$ and \vec{F} portrays the body force per unit time acting upon fluid element.

1.2.3 Conservation law of energy

Conservation law of energy states that the rate of change of kinetic and internal energies of the control volume is same as the net rate of heat input (by means of convection and conduction) and the rate of work done by the fluid on the surroundings. Mathematically:

$$\rho C_p \frac{dT}{dt} = \vec{\nabla} \cdot (k \vec{\nabla} T) + \beta T \frac{dp}{dt} + tr(\boldsymbol{\tau} \mathbf{L}), \quad (1.12)$$

where C_p stands for specific heat capacity of substance, T defines temperature of fluid, k indicates thermal conductivity, β symbolizes coefficient of thermal expansion, stress tensor and velocity gradient are indicated as $\boldsymbol{\tau}$ and \mathbf{L} respectively.

1.3 Nanofluids

Nanofluids are comprised of nano-sized particles together with base liquid. These nano-sized particles are termed as nanoparticles which consist of metals or non-metals whereas base liquids are water, oil, propylene and ethylene glycols etc. Base liquids do not possess good thermal conductivity and to cater this, nanoparticles are suspended into appropriate liquids (base liquids). Nanofluids without any doubt are the forthcoming hotspot for the researchers investigating fluids with heat transfer. Thermal power plants, medical instruments, fabrication of medicines, micro-electronic device technologies, thermal transport, paper production, heat exchangers and microelectronics are the few highlighted industrial domains for the applications of nanotechnology. Different scientists presented different models addressing the interdependence of properties of nanoparticles and base fluids.

1.3.1 Tiwari and Das model

This model relates the nanofluid properties as linear functions of base fluid properties and nanoparticles. In light of this model the conservation law of mass, conservations law of linear momentum and conservation law of energy can be expressed in following forms:

$$\left. \begin{aligned} \vec{\nabla} \cdot \mathbf{V} &= 0, \\ \rho_{nf} \left(\frac{\partial \mathbf{V}}{\partial t} + (\mathbf{V} \cdot \vec{\nabla}) \mathbf{V} \right) &= -\vec{\nabla} p + \mu_{nf} \nabla^2 \mathbf{V}, \\ \frac{\partial T}{\partial t} + (\mathbf{V} \cdot \vec{\nabla}) T &= \alpha_{nf} \nabla^2 T. \end{aligned} \right\} \quad (1.13)$$

where ρ_{nf} and μ_{nf} stands for the density and viscosity of the nanofluid while T indicates fluid's temperature. The physical quantities appearing in Eq. (1.13) were documented by different scientists and are given below:

A formula elucidating dependence of viscosity on ϕ is proposed by Brinkmann [45] :

$$\mu_{nf} = \frac{\mu_f}{(1 - \phi)^{2.5}}, \quad (1.14)$$

The expressions for effective density of nanofluid ρ_{nf} , thermal diffusivity of nanofluid α_{nf} and effective heat capacity of nanofluid are given as [4]:

$$\left. \begin{aligned} \rho_{nf} &= (1 - \phi)\rho_f + \phi\rho_{np}, \\ \alpha_{nf} &= \frac{k_{nf}}{(\rho C_p)_{nf}}, \\ (\rho C_p)_{nf} &= (1 - \phi)(\rho C_p)_f + \phi(\rho C_p)_{np}, \end{aligned} \right\} \quad (1.15)$$

A relation between solid volume fraction of nanoparticles ϕ and effective thermal conductivity of nanofluid k_{nf} is suggested by Maxwell [11]:

$$k_{nf} = k_f \frac{(k_{np} + 2k_f) + 2\phi(k_{np} - k_f)}{(k_{np}2 + k_f) - \phi(k_{np} - k_f)}, \quad (1.16)$$

where ϕ defines the solid volume fraction of nanoparticles in nanofluid, k_f and k_{np} represents the thermal conductivity of base fluid and nanoparticles respectively.

1.3.2 Buongiorno Model

Buongiorno's model is based on the theory of thermal convection and uses a two-phase approach to describe the behavior of nanofluids. The model considers the nanoparticles as a separate phase and assumes that they are dispersed randomly in the fluid. The model takes into account the buoyancy forces generated by the thermal convection in the nanofluid, as well as the particle-particle and particle-fluid interactions. The model predicts that the thermal conductivity and convective heat transfer of the nanofluid are enhanced by the presence of the nanoparticles. One of the common nanoparticles used in fabricating nanofluids is carbon nanotubes. These cylindrical carbon structures exhibit exceptional thermal conductivity and can significantly improve the heat transfer capabilities of the nanofluid. Let's delve into the remarkable properties and applications of carbon nanotubes in the realm of nanofluids, further unlocking the potential of this cutting-edge technology.

Carbon nanotubes

To escalate the thermal and chemical characteristics of the base fluid, many scientists and researchers utilized carbon nanotubes (with appropriate fluids), as they possess better thermal conductivity. Carbon nanotubes (CNTs) possess fascinating nanostructures composed entirely of carbon atoms arranged in a tubular configuration. They have a cylindrical shape, resembling a rolled-up sheet of graphene. The graphene sheet is a single layer of carbon atoms arranged in a two-dimensional honeycomb lattice, and when it rolls up into a seamless cylinder, it forms a carbon nanotube. Carbon nanotubes have been categorized w.r.t. their shapes as Single-Wall and Multi-Walls carbon nanotubes (SWCNTs and MWCNTs). Diverse utilization of CNTs corresponds to many biomedical and biological applications such as, drug delivery to body organs and cells, cancer treatments, tissues regeneration and platelet activation. CNTs are also utilized in alloys, coating and films, loudspeakers and producing optical instruments. Moreover, CNTs (Single and Multi-Walled) have favorable employment in engineering such as production of batteries, super capacitors, transistors, solar cells, electric cables and wires. Furthermore, CNTs also revolutionized water treatment systems and environmental remediation as they contribute a lot in fight against climate change.

1.4 Boundary layer flow

In a flow field, when a fluid interfaces with a solid surface during flow, formation of boundary layer comes into effect. This happens because the fluid in direct contact with the solid surface sticks to its surface due to the no-slip condition, leading to zero-velocity at the wall. As one moves away from the solid surface, the fluid velocity gradually rises through a series of layers and reaches the free stream velocity outside the boundary layer. The region where the fluid encounters most significant influence of frictional forces from the solid surface is exclusively called the boundary layer. Beyond this thin layer, the fluid maintains its original free stream

velocity, as shown in Fig. (1.2).

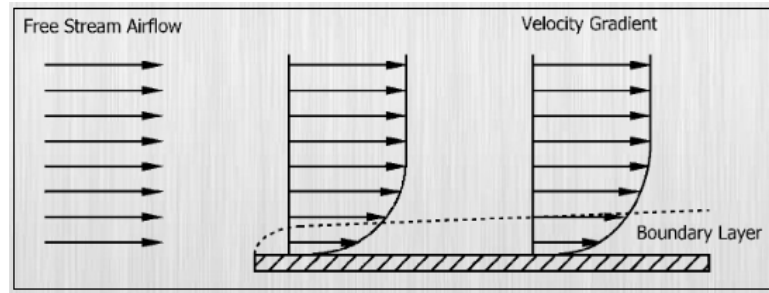


Fig. (1.2) Illustrative diagram of boundary layer formation

1.5 Some dimensionless numbers

1.5.1 Reynolds number

Reynolds number expresses the ratio of inertial force to viscous force. Mathematically, it can be portrayed as:

$$\text{Re} = \frac{\textit{inertial force}}{\textit{viscous force}} = \frac{Ul}{\nu}, \quad (1.17)$$

where characteristic length is described as l , U indicates free stream velocity and $\nu = \frac{\mu}{\rho}$ stands for kinematic viscosity. Reynolds number Re is utilized to distinguish turbulent and laminar flow descriptions. Laminar flows possess low Reynolds number ($\text{Re} < 2000$) while, turbulent flow exhibits high Reynolds number ($\text{Re} > 4000$). The fluid flows exhibiting values for Reynolds number between 2000 and 4000 are referred to as transition flows.

1.5.2 Prandtl number

Prandtl number can be signified as the ratio of momentum diffusivity to thermal diffusivity. Mathematically, Prandtl number can be depicted as:

$$\text{Pr} = \frac{\textit{Momentum diffusivity}}{\textit{Thermal diffusivity}} = \frac{\nu}{\alpha}, \quad (1.18)$$

where α and ν stand for thermal diffusivity and momentum diffusivity respectively.

1.5.3 Nusselt number

Dimensionless Nusselt number (Nu) used in heat transfer analysis to quantify the rate of convective heat transfer across boundary of solid surface. Mathematical expression for Nusselt number can be written as:

$$Nu = \frac{\text{convective heat transport}}{\text{conductive heat transport}} = \frac{hL}{k}, \quad (1.19)$$

where L expresses characteristics length, k stands for thermal conductivity and h indicates coefficient of convective heat transfer.

1.6 Heat transfer

Heat transfer governs the movement of thermal energy from regions of higher temperature to those of lower temperature to attain equilibrium. Heat transfer plays a crucial role in various natural and engineered systems, influencing everything from weather patterns and thermal comfort to the design of efficient cooling systems and heat exchangers. Three modes of heat transfer are convection, conduction and radiation.

1.6.1 Conduction

Heat conduction is a process of energy transfer that takes place within a medium, driven by the dynamic interaction of its constituent molecules. At the molecular level, conduction phenomenon arises from the collision of molecules with varying kinetic energies. When molecules with greater kinetic energy collide with particles possessing lower kinetic energy, the particles with lower kinetic energy absorbs energy, leading to an overall transfer of thermal energy across the medium. The rate of conduction is calculated as follows:

$$Q_{\text{conduction}} = \frac{kA(T_{\text{hotter}} - T_{\text{colder}})}{s}, \quad (1.20)$$

where k stands for thermal conductivity, A defines the area, s represents thickness of body, T_{hotter} and T_{colder} portray temperatures of hotter and colder regions respectively.

1.6.2 Convection

Convection is termed as the motion of fluid particles from regions with higher thermal energy towards the regions possessing lower thermal energy. The density difference of the fluid molecules is main cause for heat convection. Depending upon the nature of flow, convection exhibits three types i.e. mixed convection, natural (free) convection and forced convection. Newton's law of cooling elucidates heat transfer mechanism as:

$$Q_{convection} = Ah_f(T_w - T_s), \quad (1.21)$$

where coefficient of heat transfer is represented as h_f , T_w and T_s indicate surface temperature and surrounding temperature respectively.

1.6.3 Radiation

Radiation refers to the transmission of thermal energy through the emission and transmission of photons of light in visible and infrared portion of electromagnetic spectrum. All bodies constantly emit heat energy by the phenomenon of radiation and it does not require any medium to take place.

1.7 Methodology

1.7.1 Shooting technique

The shooting method converts the system of PDEs into a system of ordinary differential equations (ODEs) by assuming initial conditions at one end of the domain and integrating the ODEs forward until they match the boundary conditions at the other end. By iteratively adjusting the initial conditions, the shooting method seeks to find the correct values that satisfy both the boundary conditions and the original system of PDEs. This iterative approach provides a robust and efficient way to obtain numerical solutions for complex nonlinear PDE systems, making it a valuable tool in the realm of computational mathematics and engineering simulations. The NDSolve function in Mathematica is a built-in powerful numerical solver that plays a fundamental role in solving ordinary and partial differential equations (ODEs and PDEs)

within the context of shooting technique. Developed by Wolfram Research, Mathematica is a comprehensive computational software system widely utilized by researchers, engineers and mathematicians for various mathematical and symbolic computations.

1.8 Literature review

Nanofluids is a state of the art class of colloidal suspensions, that turned out to be a primary field of study which blends the wonders of nanotechnology with fluid dynamics. In contrast to conventional fluids, these fluids are composed of nanosized particles (nanoparticles) infused into a base fluid. These nanoparticles can be derived from a broad variety of substances including metals, non-metals, and metal oxides etc. whereas routine base liquids are oil, water and ethylene glycol etc. This infusion of nanoparticles into base liquid results in a versatile fluid medium featuring upgraded thermal conductivity contrary to conventional heat transfer fluids. Due to their exceptional features, nanofluids revolutionized various industries including automotive industry, electronics, energy systems and medical industry. In automotive industry nanofluids are engaged for upgrading the cooling efficiency of heat engines, improving performance of heat exchangers and radiators. In electronics and energy systems nanofluids are engaged to dissipate heat from electronic devices making them last longer. In energy storage devices nanofluids aid in effective thermal management such as enhancing the efficiency of solar panels. Moreover, in medical industry nanofluids plays in crucial role in optimizing targeted diagnostics, drug delivery and bioimaging. Due to their promising utilization in industry, fluids comprising nano-sized particles gained exceptional attention of the researchers. Choi [1] was the explorer who laid the groundwork for the evolution of nanofluids as a new category of thermal transmitted fluids. He proposed the idea that adding small amounts of nanoparticles to a fluid could dramatically enhance its thermal conductivity. Soon after this, Kim et al. [2] investigated the convective instability and heat transmission properties of nanofluids. Buongiorno [3] documented a study to explain the convective heat transmission in nanofluids. Tiwari and Das [4] examined the heat transfer performance of a square cavity filled with nanofluid under differentially heated conditions. The study also investigates the influence of the lid-driven motion on the heat transfer performance of the nanofluid. Buongiorno's work [3] was extended by Khan and Pop [5] in re-

gard to boundary layer nano-liquid flow over a stretchable sheet. The examination explored the effects of various parameters such as the stretching rate, nanoparticle volume fraction, thermal conductivity and heat transfer characteristics of the nanofluid. The heat and mass transmission phenomenon of nanofluid flow past a vertical plate under natural convection conditions were elaborated by Kuznetsov et al. [6]. Cu-H₂O based nanofluid was evaluated and documented by Raza et al. [7], by taking into account the impact of Brownian motion and thermophoresis, which are two unique properties of nanofluids. Further literature can be seen [8 – 10].

Carbon nanotubes (both single and multiple-walled) are one of the most fascinating and promising materials of our time. These incredibly small tubes are made up of carbon atoms, arranged in a unique way that creates a strong, flexible and highly conductive structure. They are so small that they are measured in nanometers or billionths of a meter. Carbon nanotubes have the strength to revolutionize a broader aspect of industries from electronics to medicine to energy. They are already being used in everything from super-strong materials to ultra-fast computer chips and scientists are constantly discovering new ways to harness their unique properties. Maxwell [11] conducted a formal investigation on carbon nanotubes, exploring their effects on electricity and magnetism. Later on, Xue [12] developed a model to predict the thermal conductivity of CNT-based composites. The model takes into account the microstructure of the composites, including the orientation, length and concentration of the CNTs as well as the thermal conductivity of the surrounding matrix material. Khan et al. [13] investigated the dynamics of Stoke's first problem for CNTs suspended nanofluids in the presence of slip boundary condition. The results of the study show that the inclusion of CNTs enhances the heat transmission rate and the skin friction coefficient, while slip boundary condition has a prominent impact on the fluid flow and heat transfer performance of the nanofluid. Hayat et al. [14] investigated the radiation effects for nanofluid flow over a rotating disk in the presence of carbon nanotubes (CNTs) and partial slip. A mathematical model to analyze the behavior of CNT-based nanomaterial flow in the presence of two coaxially circulating disks was unveiled by Khan et al. [15]. The results of the study show that the existence of CNTs enhances the heat transmission rate and reduces the occurrence of entropy, while affecting the flow and temperature fields of the nanomaterial. Acharya et al. [16] scrutinized the mixed convective flow of carbon nanotubes (CNTs) over a convectively heated curved surface. Due to the prominent

applications of carbon nanotubes many researchers tried to harness the properties of CNTs [17 – 20].

Driven by their potential to revolutionize a wide range of industry, the study of non-Newtonian fluids have become the principal subject for the researchers working in the field. When researching non-Newtonian fluids with complexity beyond Newtonian behavior, the second-grade fluid model is of utmost significance. It helps to better understand and characterize viscoelastic fluids by giving important insights about flow characteristics of substances like polymer solutions. The second-grade fluid model is crucial in various industries, including polymer processing, biomedical engineering and oil drilling, where precise fluid behavior predictions are necessary for the best design and performance. It can describe shear-thinning and shear-thickening behaviors. In recent times Hayat and Sajid [21] amplified second-grade axisymmetric fluid flow past an elastic sheet. Saif et al. [22] given thought to a stagnation point stream of a second-grade nano-material in the vicinity of non-linear extending surface with a fluctuating thickness. Hayat et al. [23] given an explanation of second-grade fluid flow across a porous surface. Radiative stream of a second-grade nanofluid overtop an extending surface was illustrated by Jamshed et al. [24]. The Stefan blowing impact was incorporated by Gowda et al. [25] to investigate the second-grade fluid flow overtop a curved elastic surface. In fluid flow systems where yield stress and viscosity are important components, the Casson fluid model is essential for understanding non-Newtonian flow behavior. Its importance is in precisely forecasting the flow properties of complicated materials like blood, pigments and specific food items. The Casson fluid model helps us better understand fluid dynamics and facilitates process optimization in a variety of sectors by taking the yield stress into consideration. S. Pramanik [26] investigated the heat transfer for Casson fluid flow of boundary layer description incorporating thermal radiation effect. Gireesha et al. [27] conducted heat and mass transfer study for MHD Casson fluid flow of boundary layer description through a permeable stretched sheet via a porous material. Ali et al. [28] investigated the impacts of multi-slip effects on the magnetohydrodynamics (MHD) time-dependent Casson nano-fluid flow passing a penetrable stretched sheet embedded in a porous medium having suction/injection thermal diffusion effect. Keeping radiation effect in mind, Nandeppanavar et al. [29] examined transfers of heat and mass of Casson fluid flow across a moving vertical plate with convective surface conditions.

M.M. Alqarni et al. [30] studied the sway of second-order chemical reaction, thermal radiation, buoyancy and heat source of a Casson fluid ovetop a circular disk and estimated its numerical solution.

Numerous real-world applications are associated with boundary-layer flow across a flexible surface in manufacturing, engineering, and industrial processes such as in the creation of paper, the processing of food, the production of fiberglass, the drawing of wires and plastic films, the condensation of liquid films, the development of crystals, the production and extraction of polymers, the fabrication of rubber sheets, etc. Moreover, several engineers and scientists are interested in designing and developing new appliances with rapid heating and cooling. Sakiadis [31] started the investigation of flow with boundary layer description due to a stretchable sheet and presented the numerical findings. Along a stretched sheet, Crane [32] investigated the 2-Dimensional (2-D) laminar flow of a incompressible viscous fluid. Several attempts have been made to realize this goal through theoretical and practical means, but all of these investigations have focused on linear and non-linear stretching of surfaces, whereas fluid flow through curved stretching surfaces has largely gone unresearched. Sajid et al. [33] were the first to provide an investigation on fluid flow with respect to a curved stretching surface. With subject to a curved elastic sheet, Saif et al. [34] illustrated the Darcy-Forchheimer flow of a viscous fluid utilizing the concept of homogenous-heterogenous reactions. Saba et al. [35] explored a 2-D boundary layer radiative flow and heat transport under the impact of internal heat generation. Rabeeah et al. [36] examined the effects of heat radiation on the incompressible steady Williamson fluid flow ovetop a curved stretching surface.

1.9 Research objectives

The primary objectives of the research are listed as:

- To compare the fluid flows owing to Casson fluid model and second-grade fluid model flowing ovetop a curved extendable surface.
- To scrutinize the impacts of carbon nanotubes on physical and thermal properties of non-Newtonian fluids, particularly Casson fluid and second-grade fluid.

- To capture the influence of thermal radiation and internal heat generation on thermal transmission.
- To investigate the influence of varying solid volume fractions of carbon nanotubes on physical properties of the base fluid.

Chapter 2

Impact of thermal radiation and internal heat generation on Casson nanofluid flowing by a curved stretchable surface with suspension of carbon nanotubes

In this chapter heat transmission of radiative nanofluid is inspected in regard to boundary layer description. Carbon nanotubes (CNTs) dependent fluid is being evaluated and it flows overtop a curved stretching surface. Special features, like thermal radiation and internal heat generation, which corresponds to heat transmission along the flow have been incorporated. Dual nature of carbon nanotubes, that is, single walled carbon nanotubes (SWCNTs) as well as multiple walled carbon nanotubes (MWCNTs) together with Casson fluid (base fluid) have been utilized for the composition of nanofluid. Appropriate transformations have been applied to reduce the modelled system of nonlinear partial differential equations into a system of ordinary differential equations (ODEs). To achieve the desired numerical solution of obtained system of ODEs, NDSolve technique is employed using Mathematica. Numerous parameters appearing in governing equations, exert influence on focused physical quantities. Graphs have been engaged to capture these variations for both SWCNTs and MWCNTs. Likewise, numeric charts have been displayed to investigate impressions on skin friction coefficient and Nusselt number for distinct parameters.

2.1 Mathematical analysis

The flow under consideration is 2-D steady incompressible nanofluid overtop a curved stretching sheet at $r_d = R_c^*$. To model the governing equations, curvilinear coordinates (r_d, s_d) have been employed. Nanofluid under inspection is produced by adding nano-sized particles of carbon nanotubes (SWCNTs and MWCNTs) to blood (base fluid). Moreover, thermal transmission phenomenon is also taken into account via internal heat generation as well as thermal radiation. Fig. (2.1) elucidates that the curved boundary being elongated in s_d direction linearly with velocity $x_s = as_d$.

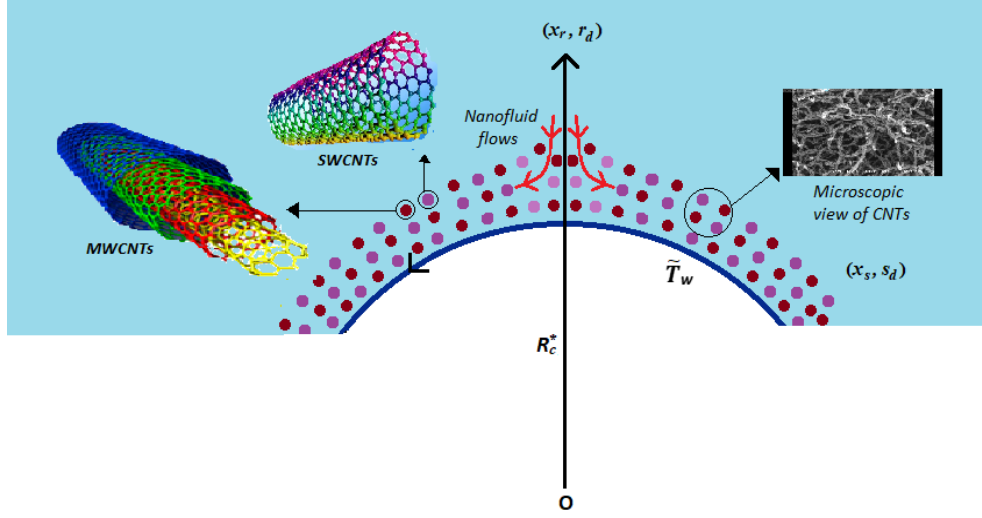


Fig. (2.1) Geometrical view of the problem

Under boundary layer approximation, the equations governing the flow are stated as:

$$\frac{\partial}{\partial r_d} ((r_d + R_c^*) x_r) + R_c^* \frac{\partial x_s}{\partial s_d} = 0, \quad (2.1)$$

$$\frac{x_s^2}{r_d + R_c^*} = \frac{1}{\rho_{nf}} \frac{\partial P}{\partial r_d}, \quad (2.2)$$

$$x_r \frac{\partial x_s}{\partial r_d} + \frac{R_c^* x_s}{r_d + R_c^*} \frac{\partial x_s}{\partial s_d} + \frac{x_s x_r}{r_d + R_c^*} = -\frac{1}{\rho_{nf}} \frac{R_c^*}{r_d + R_c^*} \frac{\partial P}{\partial s_d}$$

$$+\nu_{nf} \left(1 + \frac{1}{\beta^c}\right) \left(\frac{\partial^2 x_s}{\partial r_d^2} + \frac{1}{r_d + R_c^*} \frac{\partial x_s}{\partial r_d} - \frac{x_s}{(r_d + R_c^*)^2}\right), \quad (2.3)$$

$$\begin{aligned} x_r \frac{\partial \tilde{T}}{\partial r_d} + \frac{R_c^* x_s}{r_d + R_c^*} \frac{\partial \tilde{T}}{\partial s_d} &= \alpha_{nf} \left(\frac{\partial^2 \tilde{T}}{\partial r_d^2} + \frac{1}{r_d + R_c^*} \frac{\partial \tilde{T}}{\partial r_d}\right) \\ - \frac{1}{\rho_{nf}(r_d + R_c^*)} \frac{\partial}{\partial r_d} (r_d + R_c^*) \dot{q}_r &+ \frac{\gamma}{(\rho C_p)_{nf}} (\tilde{T} - \tilde{T}_\infty). \end{aligned} \quad (2.4)$$

The associated boundary conditions are as follows:

$$\left. \begin{aligned} x_s = a s_d, x_r = 0, \tilde{T} = \tilde{T}_w &\quad \text{at } r_d = 0, \\ x_s \rightarrow 0, \frac{\partial x_s}{\partial r_d} \rightarrow 0, \tilde{T} \rightarrow \tilde{T}_\infty &\quad \text{as } r_d \rightarrow \infty. \end{aligned} \right\} \quad (2.5)$$

where x_r and x_s are velocities in r_d and s_d directions respectively, R_c^* is the radius of curvature of curved sheet, base fluid's (Casson fluid) temperature is represented as \tilde{T} , free stream temperature is expressed as \tilde{T}_w , dimensionless pressure as P , radiative heat flux as \dot{q}_r , volumetric rate of heat generation due to heat source as γ .

Roseland's [41] approximation yields radiative heat flux term as

$$q_r = -\frac{4\sigma}{3a_R} \frac{\partial \tilde{T}^4}{\partial r_d}. \quad (2.6)$$

where a_R is the coefficient for Roseland mean approximation and σ is Stefan-Boltzmann constant. Temperature deviation is considered in such a fashion that \tilde{T}^4 can be expanded about \tilde{T}_∞ using Taylor series expansion. Ignoring higher order terms:

$$\tilde{T}^4 \approx 4\tilde{T}_\infty^3 \tilde{T} - 3\tilde{T}_\infty^4. \quad (2.7)$$

Now using Eq. (2.6) and Eq. (2.7) in Eq. (2.4) we get:

$$\begin{aligned} x_r \frac{\partial \tilde{T}}{\partial r_d} + \frac{R_c^* x_s}{r_d + R_c^*} \frac{\partial \tilde{T}}{\partial s_d} &= \frac{k_{nf}}{(\rho C_p)_{nf}} \left(1 + \frac{16\sigma^* \tilde{T}_\infty^3}{3a_R k_f (k_{nf}/k_f)}\right) \left(\frac{\partial^2 \tilde{T}}{\partial r_d^2} + \frac{1}{r_d + R_c^*} \frac{\partial \tilde{T}}{\partial r_d}\right) \\ &+ \frac{\gamma}{(\rho C_p)_{nf}} (\tilde{T} - \tilde{T}_\infty). \end{aligned} \quad (2.8)$$

Taking $R_D = \frac{16\sigma^* \tilde{T}_\infty^3}{3a_R k_f}$ as correspondence to radiation parameter, following Magyari and Pan-

tokratoras [42], Eq. (2.8) becomes:

$$x_r \frac{\partial \tilde{T}}{\partial r_d} + \frac{R_c^* x_s}{r_d + R_c^*} \frac{\partial \tilde{T}}{\partial s_d} = \frac{\nu_f}{\Delta_3 \text{Pr}} \frac{1}{k_f} \left(1 + \frac{R_D}{(k_{nf}/k_f)} \right) \left(\frac{\partial^2 \tilde{T}}{\partial r^2} + \frac{1}{r_d + R_c^*} \frac{\partial \tilde{T}}{\partial r_d} \right) + \frac{\gamma}{(\rho C_p)_{nf}} (\tilde{T} - \tilde{T}_\infty), \quad (2.9)$$

where $\text{Pr} = \frac{\nu_f}{\alpha_f}$, stands for Prandtl number. To simplify the governing equations, we employ the following similarity variables:

$$\left. \begin{aligned} x_s &= as_d f'(\zeta), x_r = -\frac{R_c^*}{r_d + R_c^*} \sqrt{a\nu_f} f(\zeta), \zeta = \sqrt{\frac{a}{\nu_f}} r_d, \\ P &= \rho a^2 s_d^2 P(\zeta), \tilde{T} = \tilde{T}_\infty + \frac{As_d}{l} \theta(\zeta), \theta(\zeta) = \frac{\tilde{T} - \tilde{T}_\infty}{\tilde{T}_w - \tilde{T}_\infty}. \end{aligned} \right\} \quad (2.10)$$

With the help of Eq. (2.10), Eq. (2.1) is trivially satisfied and Eqs. (2.2), (2.3) and (2.9) can be written as:

$$\frac{\partial P}{\partial \zeta} \frac{1}{\Delta_1} = \frac{f'^2}{\zeta + \kappa}, \quad (2.11)$$

$$\begin{aligned} &\frac{2\kappa}{\zeta + \kappa} \frac{P}{\Delta_1} - \frac{\kappa}{\zeta + \kappa} f f'' + \frac{\kappa}{\zeta + \kappa} f'^2 - \frac{\kappa}{(\zeta + \kappa)^2} f f' \\ &- \Delta_2 \left(1 + \frac{1}{\beta^c} \right) \left(f''' + \frac{1}{\zeta + \kappa} f'' - \frac{1}{(\zeta + \kappa)^2} f' \right) = 0, \end{aligned} \quad (2.12)$$

$$\left(1 + \frac{R_D}{(k_{nf}/k_f)} \right) \left(\theta'' + \frac{\theta'}{\zeta + \kappa} \right) - \frac{\text{Pr}}{(k_{nf}/k_f)} \left(\Delta_3 \frac{\kappa}{\zeta + \kappa} (f' \theta - f \theta') - \lambda_1 \theta \right) = 0, \quad (2.13)$$

where $\kappa = \sqrt{\frac{a}{\nu_f}} R_c^*$ stands for dimensionless radius of curvature and $\lambda_1 = \frac{\gamma}{a(\rho C_p)_f}$ defines heat generation parameter. Further parameters Δ_1, Δ_2 and Δ_3 are formulated as:

$$\left. \begin{aligned} \Delta_1 &= 1 - \phi + \phi \frac{\rho_{CNT}}{\rho_f}, \\ \Delta_2 &= \frac{1}{(1-\phi)^{2.5} \left(1 - \phi + \phi \frac{\rho_{CNT}}{\rho_f} \right)}, \\ \Delta_3 &= 1 - \left(1 - \frac{(\rho C_p)_{CNT}}{(\rho C_p)_f} \right) \phi. \end{aligned} \right\} \quad (2.14)$$

The utilization of Eq. (2.10) transform the boundary conditions into dimensionless form as:

$$f(0) = 0, \quad f'(0) = 1, \quad \theta(0) = 1, \quad f'(\infty) = 0, \quad f''(\infty) = 0, \quad \theta(\infty) = 0. \quad (2.15)$$

Getting rid of pressure from Eq. (14) and Eq. (15) we get:

$$\begin{aligned} & \left(1 + \frac{1}{\beta^c}\right) \left(f^{iv} + \frac{2}{\zeta + \kappa} f''' - \frac{1}{(\zeta + \kappa)^2} f'' + \frac{1}{(\zeta + \kappa)^3} f'\right) \\ & + \frac{1}{\Delta_2} \left(\frac{\kappa}{\zeta + \kappa} (f f''' - f' f'') + \frac{\kappa}{(\zeta + \kappa)^2} (f f'' - f'^2) - \frac{\kappa}{(\zeta + \kappa)^3} f f'\right) = 0, \end{aligned} \quad (2.16)$$

whereas expression for pressure can be obtained as follows:

$$P = \frac{\zeta + \kappa}{2\kappa} \Delta_1 \left(\begin{array}{l} \left(\frac{\kappa}{\zeta + \kappa} f f'' - \frac{\kappa}{\zeta + \kappa} f'^2 + \frac{\kappa}{(\zeta + \kappa)^2} f f'\right) \\ + \Delta_2 \left(1 + \frac{1}{\beta^c}\right) \left(f''' + \frac{1}{\zeta + \kappa} f'' - \frac{1}{(\zeta + \kappa)^2} f'\right) \end{array} \right). \quad (2.17)$$

Table 2.1. Thermophysical characteristics of Casson fluid and carbon nanotubes (SWCNTs and MWCNTs).

	$\rho(Kgm^{-3})$	$C_p(Jkg^{-1}K^{-1})$	$k(Wm^{-1}K^{-1})$
Casson Fluid	1053	3594	0.492
SWCNTs	2600	425	6600
MWCNTs	1600	796	3300

The skin-friction coefficient (C_f) as well as local Nusselt number (Nu_{s_d}) in s_d direction are defined as:

$$C_f = \frac{\tau_{r_d s_d}}{\rho_f u_w^2}, \quad Nu_{s_d} = \frac{s_d \dot{q}_w}{k_f (\tilde{T}_w - \tilde{T}_\infty)}, \quad (2.18)$$

where u_w is velocity in s_d -direction, $\tau_{r_d s_d}$ and \dot{q}_w describes wall shear stress as well as wall heat flux in s_d direction respectively as follows:

$$\left. \begin{aligned} \tau_{r_d s_d} &= \mu_{nf} \left(1 + \frac{1}{\beta^c}\right) \left(\frac{\partial x_s}{\partial r_d} - \frac{x_s}{r_d + R_c^*}\right) \Big|_{r_d=0}, \\ \dot{q}_w &= -k_{nf} \left(1 + \frac{16\sigma^* \tilde{T}_\infty^3}{3a_R k_f (k_{nf}/k_f)}\right) \frac{\partial \tilde{T}}{\partial r_d} \Big|_{r_d=0}. \end{aligned} \right\} \quad (2.19)$$

Upon employing Eq. (2.10) and Eq. (2.19) into Eq. (2.18) one can obtain dimensionless

expressions for skin-friction coefficient and local Nusselt number respectively as follows:

$$\left. \begin{aligned} \text{Re}_{s_d}^{1/2} C_f &= \frac{1}{(1-\phi)^{2.5}} \left(1 + \frac{1}{\beta^c} \right) \left(f''(0) - \frac{f'(0)}{\kappa} \right), \\ \text{Re}_{s_d}^{-1/2} Nu_{s_d} &= -\frac{k_{nf}}{k_f} \left(1 + \frac{R_D}{(k_{nf}/k_f)} \right) \theta'(0), \end{aligned} \right\} \quad (2.20)$$

where $\text{Re}_{s_d} = \frac{as_d^2}{\nu_f}$ expresses Reynold's number.

2.2 Numerical solution and discussion

The evaluation of the exact solution for derived non-linear system of Eqs. (2.11), (2.13) and (2.16) with boundary conditions (2.15) is a bit hard assignment. An efficient numerical technique, namely, the shooting technique via software MATHEMATICA is utilized to get the solution. Boundary value problem is converted into initial value problem with first-order differential equations with few missing initial constraints under the umbrella of this technique. These missing initial constraints are selected in such a way that they must be satisfied the asymptotic boundary conditions. Meanwhile, Table 2.1 is also utilized to evaluate Eq. (2.14) which is incorporated to evaluate the exact solution for derived non-linear system of equations. Table 2.3 is generated to assess the effectiveness and accuracy of the numerical technique employed in this study. This table guarantees the validity of employed numerical technique by showcasing that our outcomes using shooting method aligns closely with results in existing literature obtained by Runge–Kutta–Fehlberg fourth–fifth-order method. Table 2.4 serves to present a comprehensive comparison between our results and the findings in existing literature, which shows an excellent agreement. After getting the solution, this portion is compiled to investigate the actions of numerous effectual parameters including dimensionless radius of curvature (κ), Casson parameter (β^c), solid volume fraction of carbon nanotubes (ϕ), internal heat generation parameter (λ_1), radiation parameter (R_D) and Prandtl number (Pr) on velocity $f'(\zeta)$ and temperature $\theta(\zeta)$ profiles. The action of dimensionless radius of curvature (κ) on velocity profile is presented in Fig. (2.2). For higher estimation of (κ), the viscous force declines and the fluid encounters less frictional force among its particles, which allows fluid to move at higher velocity. Ultimately the velocity field increases for both single and multi-walled CNTs. The trends for velocity profile for solid volume fraction (ϕ) of carbon nanotubes is revealed in Fig. (2.3). A confident inflation

in velocity has been perceived as the solid volume fraction of CNTs is increased. Greater solid volume fraction of carbon nanotubes implies enhanced thermal conductivity of fluid, which corresponds to higher velocity of fluid. Moreover it has been recorded that SWCNTs have slightly less velocity as compared to MWCNTs due to greater density values of MWCNTs. These larger density values enhanced resistance within fluid. Therefore, the velocity for SWCNTs is lower as compared to MWCNTs. Fig. (2.4) portrays the effect of Casson parameter (β^c) on velocity profile. It can be concluded that increment in β^c causes a decline in velocity profile. Actually an increment in β^c causes higher drag force, which corresponds to slow liquid movement within the boundary layer, which is the reason of decline in fluid's velocity. Fig. (2.5) elucidates impacts of (κ) on temperature profile $\theta(\zeta)$. Physically greater values of κ reduces the viscous force (i.e. decay in fluid's kinematic viscosity), which corresponds to declination of $\theta(\zeta)$. As the fluid's kinematic viscosity decays, fluid mobility gets enhanced and it moves faster leading to thinner thermal boundary layer. This leads to improved convective heat transfer and more enhanced exchange of thermal energy between fluid and its surroundings. So declination of $\theta(\zeta)$ is certain. Action of heat generation parameter (λ_1) on temperature profile $\theta(\zeta)$ is revealed in Fig. (2.6). It is certain that increase in the values of (λ_1) causes an upsurge in temperature. Heat generation parameter (λ_1) contains heat generation coefficient. One can easily understand that increment in (λ_1) corresponds to higher value for heat generation coefficient which implies that surface temperature is greater than free stream temperature. So the heat is transferred from sheet to fluid, hence increase in temperature is quite evident. Fig. (2.7) elucidates the trends of temperature profile $\theta(\zeta)$ in consequence of higher values of the solid volume fraction (ϕ) of carbon nanotubes. It can be viewable that temperature of the fluid as well as thermal boundary layer increases by increasing (ϕ). CNTs (both single and multi-walled) carries low specific heat and higher thermal conductivity which allows them to efficiently absorb and conduct heat. So increasing their volume in nanofluid intensifies fluid's temperature significantly. Trends in Fig. (2.8) reveal the behavior of temperature profile caused by increasing the values of radiation parameter (R_D). As predicted, the fluid's temperature rises quite significantly as an increase in R_D . The radiation parameter (R_D) contains mean absorption coefficient which declines as increase in R_D consequently the heat transfer rate seems increases at every point away from sheet. When using pure blood as base fluid, it's worth noting that the Prandtl number of

blood is 21, which is very high as compared to water and other common base fluids. Prandtl number is the ratio of momentum diffusivity to thermal diffusivity that's why its larger values decline the temperature distribution. Fig. (2.9) reveals that the pressure inside the boundary layer rises as a result of an increase in dimensionless curvature (i.e. decrease in the value of κ). However, it can be noticed that pressure approaches towards zero distant from boundary. This is due to the certainty that streamlines far away from boundary adopt the same flow pattern as in case for flat stretching sheet. Moreover, one can see from Fig. (2.10) that pressure fluctuations near and far off from boundary are unimportant for the case of flat stretching surface (i.e. $\kappa = 1000$), whereas the pressure is not constant for the case of curved surface. Therefore a definite variation in pressure is recognized, extremely inside the boundary layer.

Fig. (2.11) is generated to observe the impact of dimensionless radius of curvature (κ) on skin friction coefficient for both single and multi-walled carbon nanotubes. For higher estimation of (κ), the viscous force declines and as a consequence the resisting force declines among particles. So a decrease in values for skin friction coefficient is obvious. Fig. (2.12) shows the action of dimensionless radius of curvature (κ) on local Nusselt number. It can be seen that the value for local Nusselt number increases as an increase in (κ).

Table 2.2 depicts the action of numerous parameters including Casson parameter (β^c), solid volume fraction of carbon nanotubes (ϕ), internal heat generation parameter (λ_1) and radiation parameter (R_D). As Casson parameter (β^c) contains plastic viscosity (μ_B), a rise in Casson parameter (β^c) causes a certain rise in surface drag force (C_f). So it can be deduced that augmentation of (β^c) enhances the surface drag force (C_f) for both single and multi-walled carbon nanotubes. While on the other hand augmentation of (β^c) causes a decrease in local heat flux which corresponds to lower heat transfer. So it is certain that local Nusselt number declines as an increase in Casson parameter (β^c). Furthermore, it can be noticed that an upsurge in heat generation parameter (λ_1) causes no significant change in skin friction coefficient (C_f) for both SWCNTs and MWCNTs. Heat generation parameter (λ_1) contains heat generation coefficient. One can easily perceive that upsurge in (λ_1) causes a considerable rise in heat generation. So surface temperature becomes greater than free stream temperature. Hence heat is transferred from sheet to fluid, which corresponds a rise in fluid's temperature. Due to rise in temperature of fluid declination of heat transfer is certain, which implies that rise in (λ_1)

causes a decline in local Nusselt number.

Similarly from Table 2.2, it has been perceived that rate of heat flux raises as an upsurge in radiation parameter (R_D) contains mean absorption coefficient which generates as rise in (R_D). For this reason, the heat transfer rate seems increasing at every point away from sheet. So the local Nusselt number gets amplified as an increase in radiation parameter (R_D). However, there is no significant change in skin friction coefficient due to a variation in radiation parameter (R_D). As CNTs (both single and multi-walled) carry low specific heat and higher thermal conductivity than Casson fluid (base fluid). So increasing their volume (ϕ) in nanofluid amplifies the fluid's temperature significantly. Due to rise in temperature heat flux declines. So it turns out that local Nusselt number declines as an upsurge in solid volume fraction of nanoparticles. Moreover, enhanced values for solid volume fraction (ϕ) of CNTs drives a considerable decrease in skin friction coefficient.

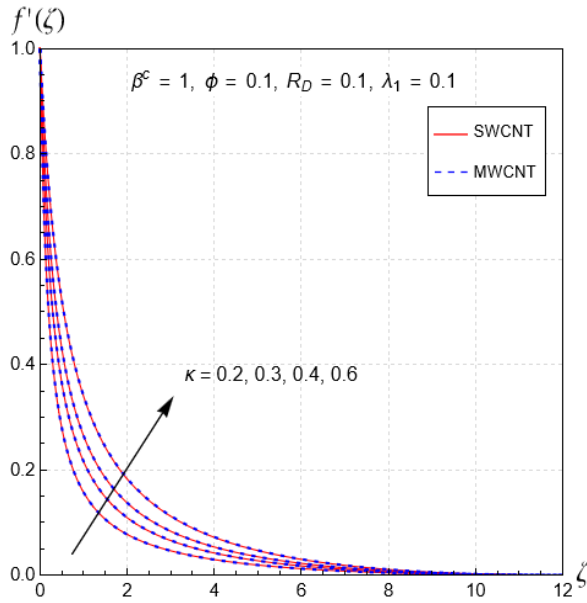


Fig. (2.2) Action of (κ) on $f'(\zeta)$

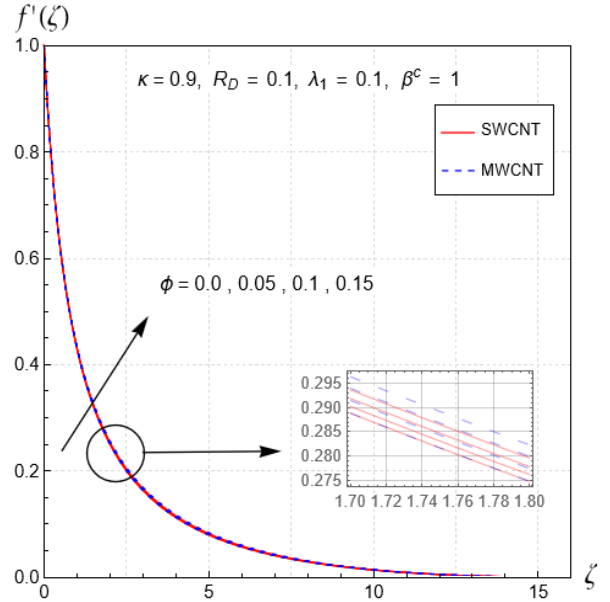


Fig. (2.3) Action of (ϕ) on $f'(\zeta)$

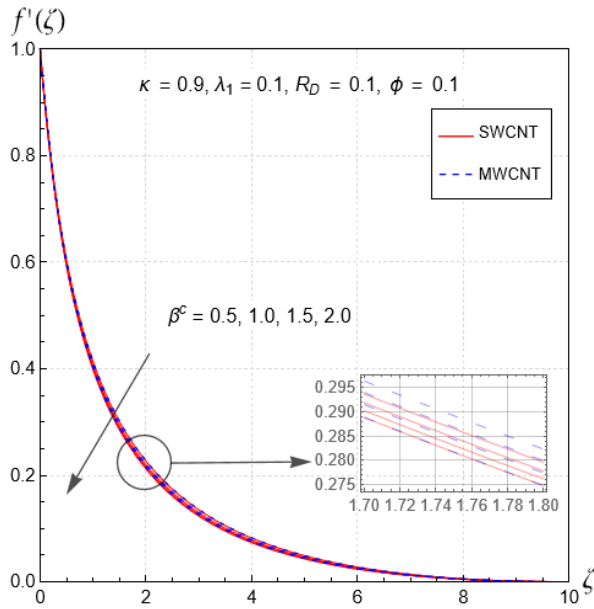


Fig. (2.4) Action of (β^c) on $f'(\zeta)$

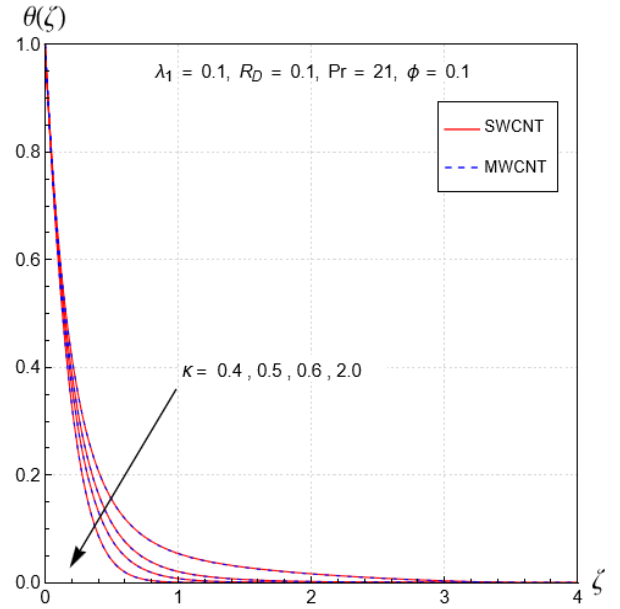


Fig. (2.5) Action of (κ) on $\theta(\zeta)$

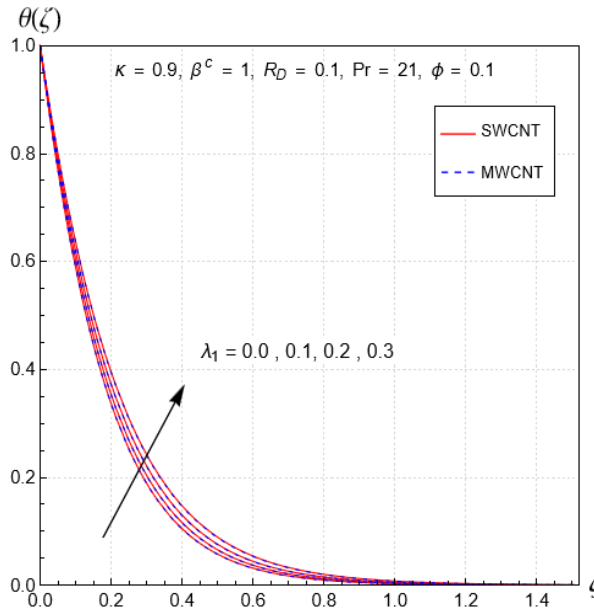


Fig. (2.6) Action of (λ_1) on $\theta(\zeta)$

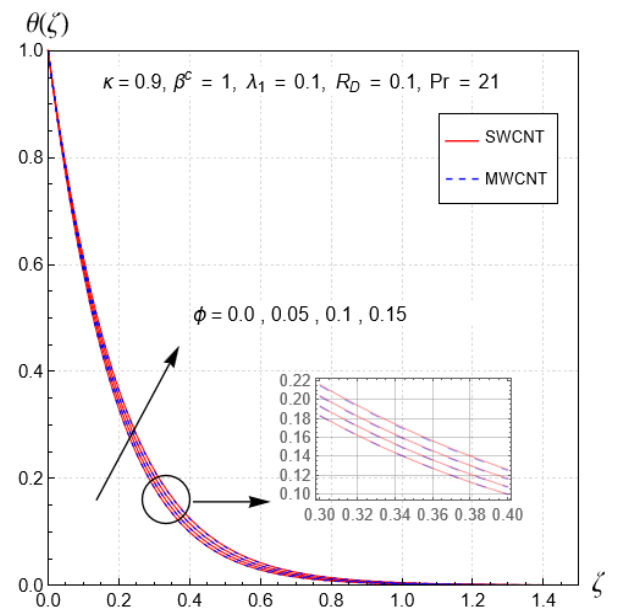


Fig. (2.7) Action of (ϕ) on $\theta(\zeta)$

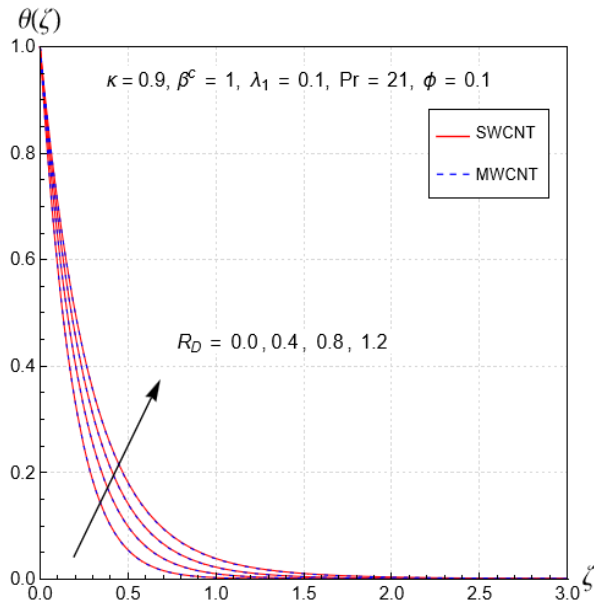


Fig. (2.8) Action of (R_D) on $\theta(\zeta)$

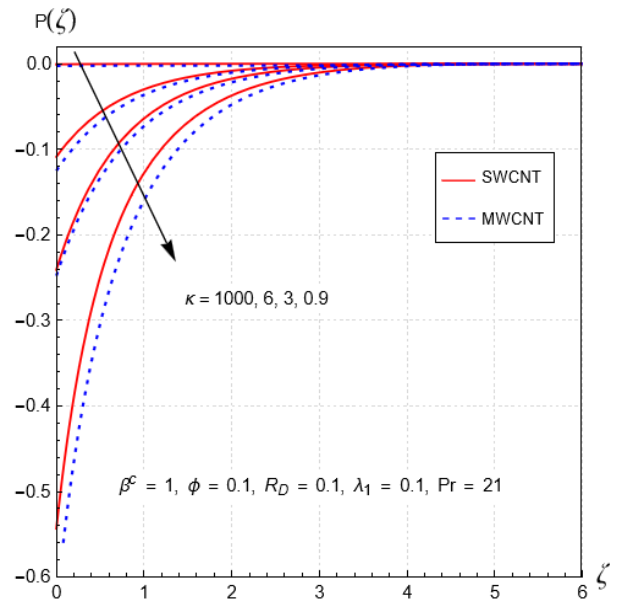


Fig. (2.9) Action of (κ) on $P(\zeta)$

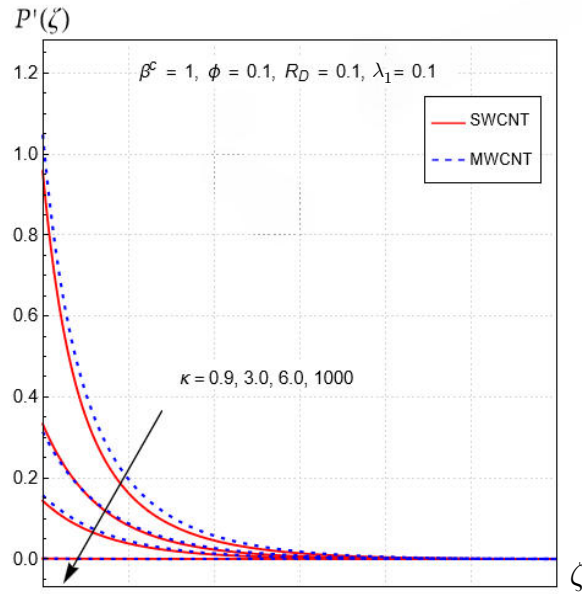


Fig. (2.10) Action of (κ) on $P'(\zeta)$

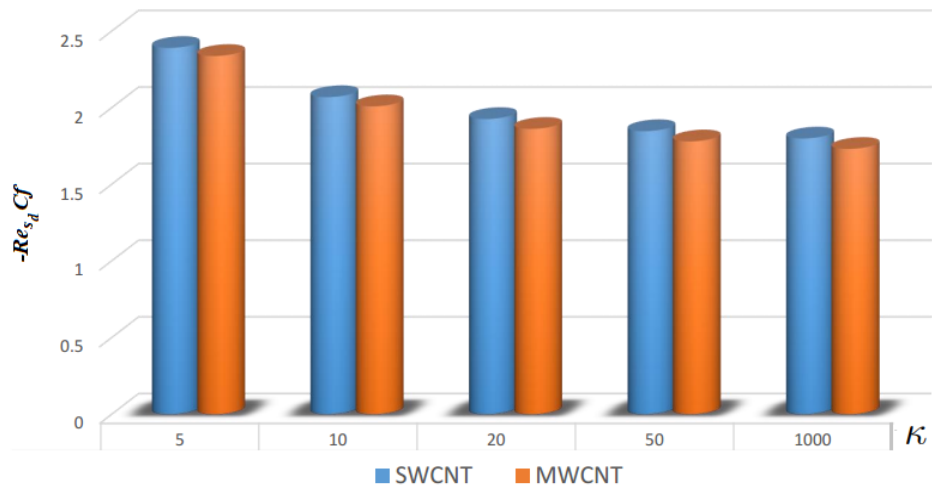


Fig. (2.11) Action of (κ) on (Cf)

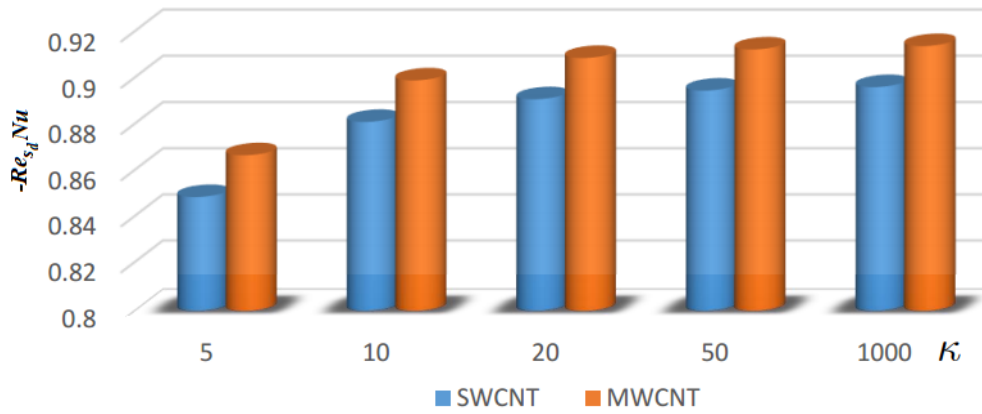


Fig. (2.12) Action of (κ) on (Nu)

Table 2.2. Numerical data for local Nusselt number and skin friction coefficient for various parameters.

ϕ	β^c	λ_1	R_D	SWCNTs		MWCNTs	
				$Re_{s_d}^{1/2} C_f$	$Re_{s_d}^{-1/2} Nu_{s_d}$	$Re_{s_d}^{1/2} C_f$	$Re_{s_d}^{-1/2} Nu_{s_d}$
0.1	1	0.1	0.1	-2.38323	1.04614	-2.33355	1.0567
0.2				-3.07012 ↓	1.01474 ↓	-2.96891 ↓	1.03364 ↓
0.3				-4.09148 ↓	0.983947 ↓	-3.93757 ↓	1.00957 ↓
0.4				-5.72829	0.953411	-5.52152	0.984876
0.1	1	0.1	0.1	-2.38323	1.04614	-2.33355	1.0567
	1.5			-2.08439 ↑	1.03143 ↓	-2.03532 ↑	1.04305 ↓
	2			-1.93374 ↑	1.02182 ↓	-1.88596 ↑	1.0341 ↓
	2.5			-1.84278	1.01506	-1.79557	1.0278
0.1	1	0.1	0.1	-2.38323	1.04614	-2.33355	1.0567
		0.2		-2.38323 —	0.952682 ↓	-2.33355 —	0.965403 ↓
		0.3		-2.38323 —	0.826032 ↓	-2.33355 —	0.843538 ↓
		0.4		-2.38323	0.600795	-2.33355	0.635055
0.1	1	0.1	0.1	-2.38323	1.04614	-2.33355	1.0567
		0.3		-2.38323 —	1.11794 ↑	-2.33355 —	1.12947 ↑
		0.5		-2.38323 —	1.18451 ↑	-2.33355 —	1.19687 ↑
		0.7		-2.38323	1.2475	-2.33355	1.26055

Table 2.3. Error analysis of the values of $-Re_{s_d}^{1/2} C_f$ to address the validity of numerical method with $R_D = \beta^c = \lambda_1 = 0$.

ϕ	κ	Nagaraja et al. [44]	Current study		Percentage relative absolute difference
			SWCNTs	MWCNTs	
0.0	5	1.15764	1.15763	1.15763	0.000864%
	10	1.07349	1.07349	1.07349	0%
	30	1.02352	1.02353	1.02353	0.000977%
	50	1.01407	1.01405	1.01405	0.001972%

Table 2.4. Comparative analysis of the values of $-\text{Re}_{s_d}^{1/2} C_f$ for distinct numerics of κ and ϕ with $R_D = \lambda_1 = 0$ and $\beta^c \rightarrow 0$.

		Abbas et al. [43]	Saba et al. [35]		Current study	
ϕ	κ		SWCNTs	MWCNTs	SWCNTs	MWCNTs
0.0	5	1.15763	1.15763	1.15763	1.15763	1.15763
	10	1.07349	1.07349	1.07349	1.07349	1.07349
	50	1.01405	1.01405	1.01405	1.01405	1.01405
	1000	1.00079	1.00079	1.00079	1.00079	1.00079
0.1	5	–	1.43781	1.38677	1.43707	1.38669
	10	–	1.32577	1.27251	1.32569	1.27247
	50	–	1.27579	1.22190	1.27549	1.22186

2.3 Conclusions

This exploration consists the heat transmission through a radiative flow of boundary layer description together with internal heat generation of Casson nanofluid comprised of carbon nanotubes (SWCNTs and MWCNTs) overtop a curved stretching sheet. Featured points are listed as follow:

- The velocity profile $f'(\zeta)$ rises as an increase in solid volume fraction (ϕ) and dimensionless radius of curvature (κ) whereas an opposite trend is noticed for higher values of Casson parameter (β^c).
- The temperature of fluid $\theta(\zeta)$ rises due to rise in heat generation parameter (λ_1), solid volume fraction (ϕ) and radiation parameter (R_D) however a reverse behavior is seen for varying values of dimensionless radius of curvature (κ).
- For higher values of dimensionless radius of curvature (κ) opposite action is noticed for skin friction coefficient and local Nusselt number for both single and multi-walled carbon nanotubes.
- The skin friction coefficient diminishes due to rise in dimensionless radius of curvature (κ) and solid volume fraction (ϕ) for both CNTs whereas an opposite trend is noticed

for higher values of Casson parameter (β^c) and it remains invariant for different values of heat generation parameter (λ_1) and radiation parameter (R_D)

- Local Nusselt number diminishes for higher values of Casson parameter (β^c), internal heat generation parameter (λ_1) and solid volume fraction (ϕ) however a reverse trend is noticed for dimensionless radius of curvature (κ) and radiation parameter (R_D).

Chapter 3

Second-grade fluid with carbon nanotubes flowing over a curved stretchable surface possessing thermal radiation and internal heat generation effects

In this chapter heat transmission of radiative nanofluid with reference to boundary layer nature is analyze. Carbon nanotubes (CNTs) reliant liquid is being tested and it flows on top of a curved extending surface. To scrutinize thermal transmission through the flow additional impacts of thermal radiation as well as internal heat generation have been incorporated. Dual nature of CNTs, that is, single-walled CNTs (SWCNTs) and multi-walled CNTs (MWCNTs) have been employed in conjunction with slurry mixture (base fluid) for the formulation of nanofluid. Second-grade fluid model is deployed to capture the rheological properties of nanofluid. To acquire the numerical solution of designed mathematical model, NDSolve approach is engaged using software Mathematica. Various parameters occurring in governing equations makes an impact on focused physical quantities. Graphs have been employed to capture these impacts for both SWCNTs and MWCNTs. In like manner the impact of numerous factors on skin friction coefficient as well as Nusselt number have been examined using numerical charts.

3.1 Mathematical analysis

The flow under inspection is 2D-steady incompressible flow ovetop a curved extending sheet at $r_d = R_c^*$. Curvilinear coordinates have been engaged to model the governing equations. Nanofluid being studied is composed by introducing nano-sized particles of carbon nanotubes

(SWCNTs and MWCNTs) to second grade fluid (base fluid). Moreover effects of internal heat generation and thermal radiation have also been utilized to inspect the process of thermal transmission. The curved sheet is being stretched linearly in s_d direction with velocity $x_s = as_d$, where $a > 0$ is the stretching constant. The free stream temperature and sheet's temperature are represented as T_∞ and \tilde{T}_w respectively.

The second-grade fluid possess an extra stress tensor [24] defined as

$$\boldsymbol{\tau} = -p\mathbf{I} + \mu\mathbf{A}_1 + \alpha_1\mathbf{A}_2 + \alpha_2\mathbf{A}_1^2, \quad (3.1)$$

where p denotes pressure, \mathbf{I} indicates identity tensor, μ is dynamic viscosity, $\alpha_j (j = 1, 2)$ are second grade material constants and the first two Rivlin-Ericksen tensors \mathbf{A}_1 and \mathbf{A}_2 are described as

$$\left. \begin{aligned} \mathbf{A}_1 &= (\text{grad } \mathbf{V})^t + (\text{grad } \mathbf{V}), \\ \mathbf{A}_2 &= \mathbf{A}_1(\text{grad } \mathbf{V}) + \frac{d\mathbf{A}_1}{dt} + (\text{grad } \mathbf{V})^t\mathbf{A}_1, \end{aligned} \right\} \quad (3.2)$$

in which d/dt is material time derivative and \mathbf{V} is the velocity vector. This fact should be noticed that when $\alpha_1 = \alpha_2 = 0$, the fundamental equation for second grade fluid reduces to that of viscous fluid. Employing the above assumption under boundary layer approximation, the equations that govern the flow are expressed as:

$$\frac{\partial}{\partial r_d} ((r_d + R_c^*)x_r) + R_c^* \frac{\partial x_s}{\partial s_d} = 0, \quad (3.3)$$

$$\frac{x_s^2}{r_d + R_c^*} = \frac{1}{\rho_{nf}} \frac{\partial P}{\partial r_d}, \quad (3.4)$$

$$\begin{aligned} x_r \frac{\partial x_s}{\partial r_d} + \frac{R_c^* x_s}{r_d + R_c^*} \frac{\partial x_s}{\partial s_d} + \frac{x_s x_r}{r_d + R_c^*} &= -\frac{1}{\rho_{nf}} \frac{R_c^*}{r_d + R_c^*} \frac{\partial P}{\partial s_d} + \nu_{nf} \left(\frac{\partial^2 x_s}{\partial r_d^2} + \frac{1}{r_d + R_c^*} \frac{\partial x_s}{\partial r_d} - \frac{x_s}{(r_d + R_c^*)^2} \right) \\ &+ \frac{\alpha_1}{\rho_{nf}} \left(\frac{2R_c^*}{r_d + R_c^*} \frac{\partial^2 x_s}{\partial r_d^2} \frac{\partial x_s}{\partial s_d} - \frac{2R_c^*}{(r_d + R_c^*)^2} \frac{\partial x_s}{\partial r_d} \frac{\partial x_s}{\partial s_d} + \frac{2}{r_d + R_c^*} x_r \frac{\partial^2 x_s}{\partial r_d^2} \right. \\ &\left. - \frac{2}{(r_d + R_c^*)^2} x_r \frac{\partial x_s}{\partial r} - \frac{4R_c^*}{(r_d + R_c^*)^2} x_s \frac{\partial^2 x_s}{\partial r_d \partial s_d} - \frac{4x_s}{(r_d + R_c^*)^2} \frac{\partial x_r}{\partial r_d} + \frac{2R_c^*}{(r_d + R_c^*)^3} x_s \frac{\partial x_s}{\partial s_d} \right), \end{aligned} \quad (3.5)$$

$$x_r \frac{\partial \tilde{T}}{\partial r_d} + \frac{R_c^* x_s}{r_d + R_c^*} \frac{\partial \tilde{T}}{\partial s_d} = \alpha_{nf} \left(\frac{\partial^2 \tilde{T}}{\partial r_d^2} + \frac{1}{r_d + R_c^*} \frac{\partial \tilde{T}}{\partial r_d} \right) - \frac{1}{\rho_{nf}(r_d + R_c^*)} \frac{\partial}{\partial r_d} (r_d + R_c^*) q_r + \frac{\dot{\gamma}}{(\rho C_p)_{nf}} (\tilde{T} - \tilde{T}_\infty). \quad (3.6)$$

The associated constraints are as follows:

$$\left. \begin{aligned} x_s = a s_d, x_r = 0, \tilde{T} = \tilde{T}_w & \quad \text{at } r_d = 0 \\ x_s \rightarrow 0, \frac{\partial x_s}{\partial r_d} \rightarrow 0, \tilde{T} \rightarrow \tilde{T}_\infty & \quad \text{as } r_d \rightarrow \infty \end{aligned} \right\} \quad (3.7)$$

where x_r and x_s are velocities along r_d and s_d directions respectively, for the curved sheet R_c^* indicates its radius of curvature, \tilde{T} stands for base fluid's (second grade fluid) temperature, P for dimensionless pressure, q_r for radiative heat flux, γ for rate of volumetric heat generation caused by heat source.

The term for radiative heat flux is estimated by Rooseland's approximation [41] as:

$$q_r = - \frac{4\sigma^*}{3a_R} \frac{\partial \tilde{T}^4}{\partial r_d} \quad (3.8)$$

where a_R denotes the coefficient for Rooseland mean approximation and σ is Stefan-Boltzmann constant. Temperature variation is taken into account in such fashion that \tilde{T}^4 can be expanded about \tilde{T}_∞ using Taylor series expansion while omitting terms of higher order:

$$\tilde{T}^4 \approx 4\tilde{T}_\infty^3 \tilde{T} - 3\tilde{T}_\infty^4 \quad (3.9)$$

Now using Eq. (3.8) and Eq. (3.9) in Eq. (3.6) we get:

$$\begin{aligned} x_r \frac{\partial \tilde{T}}{\partial r_d} + \frac{R_c^* x_s}{r_d + R_c^*} \frac{\partial \tilde{T}}{\partial s_d} &= \frac{k_{nf}}{(\rho C_p)_{nf}} \left(1 + \frac{16\sigma^* \tilde{T}_\infty^3}{3a_R k_f (k_{nf}/k_f)} \right) \left(\frac{\partial^2 \tilde{T}}{\partial r_d^2} + \frac{1}{r_d + R_c^*} \frac{\partial \tilde{T}}{\partial r_d} \right) \\ &+ \frac{\gamma}{(\rho C_p)_{nf}} (\tilde{T} - \tilde{T}_\infty) \end{aligned} \quad (3.10)$$

Taking $R_D = \frac{16\sigma^* \tilde{T}_\infty^3}{3a_R k_f}$ as radiation parameter [42], Eq. (3.10) takes the form:

$$\begin{aligned}
x_r \frac{\partial \tilde{T}}{\partial r_d} + \frac{R_c^* x_s}{r_d + R_c^*} \frac{\partial \tilde{T}}{\partial s_d} &= \frac{\nu_f}{\Delta_3} \frac{1}{\text{Pr}} \frac{k_{nf}}{k_f} \left(1 + \frac{R_D}{(k_{nf}/k_f)} \right) \left(\frac{\partial^2 \tilde{T}}{\partial r_d^2} + \frac{1}{r_d + R_c^*} \frac{\partial \tilde{T}}{\partial r_d} \right) \\
&+ \frac{\gamma}{(\rho C_p)_{nf}} (\tilde{T} - \tilde{T}_\infty)
\end{aligned} \tag{3.11}$$

where $\text{Pr} = \frac{\nu_f}{\alpha_f}$, symbolizes Prandtl number. To simplify the governing equations, we engage the following similarity variables:

$$\left. \begin{aligned}
x_s &= a s_d f'(\varsigma), x_r = -\frac{R_c^*}{r_d + R_c^*} \sqrt{a \nu_f} f(\varsigma), \varsigma = \sqrt{\frac{a}{\nu_f}} r_d \\
P &= \rho a^2 s_d^2 P(\varsigma), \tilde{T} = \tilde{T}_\infty + \frac{A s_d}{l} \theta(\varsigma), \theta(\varsigma) = \frac{\tilde{T} - \tilde{T}_\infty}{\tilde{T}_w - \tilde{T}_\infty}
\end{aligned} \right\} \tag{3.12}$$

With the help of Eq. (3.12), Eq. (3.3) is trivially satisfied and Eq. (3.4), Eq. (3.5) and Eq. (3.11) can be written as:

$$\frac{\partial P}{\partial \varsigma} \frac{1}{\Delta_1} = \frac{f'^2}{\varsigma + \kappa} \tag{3.13}$$

$$\begin{aligned}
\frac{2\kappa}{\varsigma + \kappa} \frac{P}{\Delta_1} - \frac{\kappa}{\varsigma + \kappa} f f'' + \frac{\kappa}{\varsigma + \kappa} f'^2 - \frac{\kappa}{(\varsigma + \kappa)^2} f f' - \Delta_2 \left(f''' + \frac{1}{\varsigma + \kappa} f'' - \frac{1}{(\varsigma + \kappa)^2} f' \right) \\
- \frac{\alpha_1}{\Delta_1} \frac{a}{\mu_f} \left(-\frac{2\kappa}{(\varsigma + \kappa)^2} (f f'' + 4f' f''') + \frac{2\kappa}{\varsigma + \kappa} f' f''' \right. \\
\left. + \frac{2\kappa}{(\varsigma + \kappa)^3} (2f'' + 3f'^2) - \frac{4\kappa}{(\varsigma + \kappa)^4} f f' \right) = 0
\end{aligned} \tag{3.14}$$

$$\left(1 + \frac{R_D}{(k_{nf}/k_f)} \right) \left(\theta'' + \frac{\theta'}{\varsigma + \kappa} \right) - \frac{\text{Pr}}{(k_{nf}/k_f)} \left(\Delta_3 \frac{\kappa}{\varsigma + \kappa} (f' \theta - f \theta') - \lambda_1 \theta \right) = 0 \tag{3.15}$$

where $\kappa = \sqrt{\frac{a}{\nu_f}} R_c^*$ symbolizes dimensionless radius of curvature and $\lambda_1 = \frac{\gamma}{a(\rho C_p)_f}$ stands for heat generation parameter. Further parameters Δ_1, Δ_2 and Δ_3 are formulated as:

$$\left. \begin{aligned}
\Delta_1 &= 1 - \phi + \phi \frac{\rho_{CNT}}{\rho_f}, \\
\Delta_2 &= \frac{1}{(1-\phi)^{2.5} \left(1 - \phi + \phi \frac{\rho_{CNT}}{\rho_f} \right)}, \\
\Delta_3 &= 1 - \left(1 - \frac{(\rho C_p)_{CNT}}{(\rho C_p)_f} \right) \phi.
\end{aligned} \right\} \tag{3.16}$$

The utilization of Eq. (3.12) transforms Eq. (3.7) into dimensionless form as:

$$\left. \begin{aligned} f(0) = 0, f'(0) = 1, \theta(0) = 1, \\ f'(\infty) = 0, f''(\infty) = 0, \theta(\infty) = 0. \end{aligned} \right\} \quad (3.17)$$

Getting rid of pressure from Eq. (3.13) and Eq. (3.14) we get:

$$\begin{aligned} & \Delta_2 \left(f^{iv} + \frac{1}{(\zeta + \kappa)^3} f' - \frac{1}{(\zeta + \kappa)^2} f'' + \frac{2}{\zeta + \kappa} f''' \right) \\ & + \frac{\kappa}{\zeta + \kappa} (f f''' - f' f'') + \frac{\kappa}{(\zeta + \kappa)^2} (f f'' - f'^2) - \frac{\kappa}{(\zeta + \kappa)^3} f f' \\ & + \frac{\alpha_1}{\Delta_1} \frac{a}{\mu_f} \left(\frac{2\kappa}{\zeta + \kappa} (f' f^{iv} + f'' f''') - \frac{10\kappa}{(\zeta + \kappa)^2} f' f''' - \frac{2\kappa}{(\zeta + \kappa)^2} f f^{iv} - \frac{8\kappa}{(\zeta + \kappa)^2} f''^2 \right. \\ & \left. + \frac{6\kappa}{(\zeta + \kappa)^3} f f''' + \frac{24\kappa}{(\zeta + \kappa)^3} f' f'' - \frac{16\kappa}{(\zeta + \kappa)^4} f'^2 - \frac{12\kappa}{(\zeta + \kappa)^4} f f'' + \frac{12\kappa}{(\zeta + \kappa)^5} f f' \right) = 0 \end{aligned} \quad (3.18)$$

Ultimately, pressure P can be obtained as follows:

$$P = \Delta_1 \frac{\zeta + \kappa}{2\kappa} \left(\begin{aligned} & \frac{\kappa}{\zeta + \kappa} f f'' - \frac{\kappa}{\zeta + \kappa} f'^2 + \frac{\kappa}{(\zeta + \kappa)^2} f f' + \Delta_2 \left(f''' + \frac{1}{\zeta + \kappa} f'' - \frac{1}{(\zeta + \kappa)^2} f' \right) \\ & - \frac{\alpha_1}{\Delta_1} \frac{a}{\mu_f} \left(\begin{aligned} & - \frac{2\kappa}{(\zeta + \kappa)^2} (f f''' + 4f' f'') + \frac{2\kappa}{\zeta + \kappa} f' f''' \\ & + \frac{2\kappa}{(\zeta + \kappa)^3} (2f'' + 3f'^2) - \frac{4\kappa}{(\zeta + \kappa)^4} f f' \end{aligned} \right) \end{aligned} \right) \quad (3.19)$$

Table 3.1. Thermophysical characteristics of carbon nanotubes (SWCNTs and MWCNTs) are tabulated as:

	$\rho(Kgm^{-3})$	$C_p(Jkg^{-1}K^{-1})$	$k(Wm^{-1}K^{-1})$
SWCNTs	2600	425	6600
MWCNTs	1600	796	3300

In s_d -direction, the skin-friction coefficient (C_f) as well as local Nusselt number (Nu_{s_d}) are defined as:

$$C_f = \frac{\tau_{r_d s_d}}{\rho_f u_w^2}, \quad Nu_{s_d} = \frac{(s_d q_w)/k_f}{(\tilde{T}_w - \tilde{T}_\infty)} \quad (3.20)$$

where u_w is velocity in s_d -direction, $\tau_{r_d s_d}$ and \dot{q}_w describes shear stress as well as heat flux at curved stretchable surface in s_d -direction respectively as follows:

$$\left. \begin{aligned} \tau_{r_d s_d} &= \frac{1}{(1-\phi)^{2.5}} \mu_{nf} \left(\frac{\partial x_s}{\partial r_d} - \frac{x_s}{r_d + \hat{R}_c^*} + \frac{2\alpha_1}{\mu_{nf}} \left(\frac{x_r}{r_d + \hat{R}_c^*} \frac{\partial x_s}{\partial r_d} + \frac{\hat{R}_c^*}{r_d + \hat{R}_c^*} \frac{\partial x_s}{\partial r_d} \frac{\partial x_s}{\partial s_d} \right) \right) \Bigg|_{r_d=0}, \\ q_w &= -k_{nf} \left(1 + \frac{16\sigma^* \tilde{T}_\infty^3}{3a_R k_f (k_{nf}/k_f)} \right) \frac{\partial \tilde{T}}{\partial r_d} \Bigg|_{r_d=0} \end{aligned} \right\} \quad (3.21)$$

Employing Eq. (3.12) in Eq. (3.20) and Eq. (3.21) we get expressions for skin-friction coefficient as well as local Nusselt number as:

$$\left. \begin{aligned} Re_{s_d}^{1/2} C_f &= \frac{1}{(1-\phi)^{2.5}} 2 \left(f''(0) - \frac{f'(0)}{\kappa} + \alpha_1 \left(-2 \frac{f'(0)^2}{\kappa} + f'(0) f''(0) \right) \right), \\ Re_{s_d}^{-1/2} Nu_{s_d} &= -\frac{k_{nf}}{k_f} \left(1 + \frac{R_D}{(k_{nf}/k_f)} \right) \theta'(0) \end{aligned} \right\} \quad (3.22)$$

where $Re_{s_d} = \frac{a s_d^2}{\nu_f}$ expresses local Reynolds number.

3.2 Numerical solution and discussion

The assessment of exact solution for the resultant system of non-linear Eqs. (3.13), (3.15) and (3.18) together with boundary conditions (3.17) is a tedious task. A well systematic technique namely, shooting method is engaged using software MATHEMATICA to get the numerical solution. Under the aegis of this approach, a boundary value problem (BVP) is transformed into an initial value problem (IVP) with first-order differential equations with a

minimal number of lacking initial constraints. These lacking initial constraints are selected in such a way that they must satisfy the asymptotic boundary constraints. Table 3.3 is generated to assess the effectiveness and accuracy of the numerical technique employed in this study. This table guarantees the validity of employed numerical technique by showcasing that our outcomes using shooting method aligns closely with results in existing literature obtained by Runge–Kutta–Fehlberg fourth–fifth-order method. Table 3.4 serves to present a comprehensive comparison between our results and the findings in existing literature, which shows an excellent agreement. After achieving the solution, this section is compiled to explore the effects of numerous parameters including dimensionless curvature (κ), solid volume fraction of CNTs (ϕ), heat generation parameter (λ_1), radiation parameter (R_D) and Prandtl number (Pr) on focused physical quantities i.e. velocity $f'(\zeta)$ and temperature $\theta(\zeta)$ of fluid. The value for Prandtl number for slurry mixture is chosen to be 5.83. The effect of dimensionless curvature (κ) on fluid's velocity $f'(\zeta)$ is unveiled in Fig. (3.1). It can be seen that an upsurge in values of dimensionless curvature (κ) causes a decline in fluid's velocity $f'(\zeta)$. This is due to the fact that value of κ determines the flow regime in curved surface. For low values of κ ($\kappa \ll 1$), the flow is considered to be in the "low-curvature" regime, where the effects of curvature are negligible. However, for high values of κ ($\kappa \gg 1$), the flow is in the "high-curvature" regime, where curvature has a significant influence on the flow behavior. The influence of solid volume fraction (ϕ) of CNTs on velocity profile $f'(\zeta)$ of nanofluid is unveiled in Fig. (3.2). A certain inflation has been noticed as the solid volume fraction (ϕ) of CNTs is increased. As the solid volume fraction (ϕ) of CNTs in the fluid increases, the number of collisions between the nanotubes and the fluid molecules also increases. These collisions cause the nanoparticles to move around in a random manner, which is known as the Brownian motion effect. This random movement of the nanoparticles creates a more chaotic environment for the fluid molecules, thereby enhancing their velocity. Moreover it has been noted that SWCNTs have slightly less velocity as compared to MWCNTs due to greater density values of MWCNTs. Fig. (3.3) portrays the influence of second-grade fluid parameter (α_1) over fluid's velocity $f'(\zeta)$. As the second-grade fluid parameter gets amplified, the velocity rises. This is because the added elasticity of the fluid can enhance its ability to resist deformation under shear. The fluid's higher elasticity allows it to absorb and store more energy, resulting in greater momentum

transfer and increased velocity. Fig. (3.4) elucidates the impact of dimensionless curvature (κ) on temperature profile $\theta(\zeta)$. Physically larger values of (κ) corresponds to reduction in viscous force (i.e. decay in kinematic velocity of fluid). Decay in kinematic viscosity of fluid corresponds to lower heat transfer. Hence a declination in temperature profile $\theta(\zeta)$ is certain. Fig. (3.5) unveils the action of solid volume fraction (ϕ) of CNTs on temperature profile $\theta(\zeta)$. Carbon nanotubes (both single and multiple-walled) have relatively greater thermal conductivity and lesser specific heat than base fluid (second grade fluid). So increasing their volume (ϕ) in nanofluid will cause a rise in $\theta(\zeta)$. Moreover as the volume fraction (ϕ) of carbon nanotubes in the fluid increases, the movement of fluid molecules becomes more restricted and the frictional forces between the fluid and the solid particles increase. This increase in frictional forces results in an increase in heat generation, which raises the temperature of the fluid. Additionally, carbon nanotubes themselves can absorb heat and transfer it to the surrounding fluid, which can further increase the temperature. Action on temperature profile $\theta(\zeta)$ by heat generation parameter (λ_1) elucidates Fig. (3.6). The heat generation parameter (λ_1) is a measure of the amount of energy being generated per unit volume of the fluid. As the heat generation parameter (λ_1) increases, the amount of energy being generated per unit volume of the fluid also increases. This leads to an increase in the amount of heat energy transferred to the fluid, causing the temperature $\theta(\zeta)$ of the fluid to rise. Fig. (3.7) depicts the sway of radiation parameter (R_D) on temperature of fluid $\theta(\zeta)$. As predicted, the fluid's temperature amplifies quite significantly as an upsurge in (R_D). The radiation parameter (R_D) comprises mean absorption coefficient which reduces as increase in (R_D) consequently the heat transfer rate seems increases at every point away from sheet. Hence an increase in fluid's temperature is certain. The effect of dimensionless curvature (κ) on pressure profile $P(\zeta)$ is explained in Fig. (3.8). One can notice that an increment in value of (κ) causes an upsurge in pressure inside the boundary layer. However pressure approaches to zero far away from the boundary. This is because as we move far from boundary the stream lines of fluid flow conduct the same manner as for the case of flat stretching surface. Moreover it Fig. (3.9) guarantees that pressure variations can be neglected throughout the flow for the case ($\kappa = 1000$) i.e. a flat stretching sheet, while it can not be neglected for curved surfaces.

Fig. (3.10) shows the impact of dimensionless curvature over skin friction coefficient (C_f). An amplification in dimensionless curvature (κ) leads to a rise in skin friction coefficient (C_f) in

a flow over a curved stretching surface due to the increased surface area of the curved surface. As the dimensionless curvature (κ) of the surface rises, the surface area also gets broadened, which can lead to a higher skin friction coefficient (C_f). This is due to the fact that the fluid molecules in contact with the surface experience a higher shear stress as the dimensionless curvature (κ) rises, resulting in a boost in skin friction coefficient (C_f). Fig. (3.11) portrays the influence of dimensionless curvature (κ) over local Nusselt number (Nu_{s_d}). As the dimensionless curvature of the surface rises (κ), the surface area also expands, which can lead to a rise in the convective heat transfer coefficient and, subsequently, an increment in the local Nusselt number (Nu_s). Additionally, the boundary layer thickness drops as the dimensionless curvature (κ) of the surface rises, resulting in an increment in heat transfer rate at the surface, which can also contribute to a rise in the local Nusselt number (Nu_s). Table 3.2 displays how several factors such as solid volume fraction of carbon nanotubes (ϕ), radiation parameter (R_D) and internal heat generation parameter (λ_1) affects skin-friction coefficient (C_f) and local Nusselt number (Nu_{s_d}). An increment in solid volume fraction of carbon nanotubes (ϕ) reduces the skin friction coefficient (C_f) due to the unique properties of carbon nanotubes. These properties, such as their high aspect ratio and excellent thermal conductivity enhances the transfer of heat and momentum in the fluid which leads to a reduction in skin friction coefficient (C_f). When the second-grade fluid parameter (α_1) is higher, fluid's viscosity tends to decrease with increasing shear rate. This decrease in viscosity with shear rate is known as shear-thinning behavior. The shear-thinning behavior of the second-grade fluid leads to the reduction in the effective viscosity near the surface, resulting in decline of skin friction coefficient (C_f). Furthermore thermal radiation (R_D) and internal heat generation (λ_1) do not change the value of the local skin friction coefficient (C_f) because they do not directly affect the shear stress at the surface. Skin friction coefficient is the ratio of shear stress to the dynamic pressure of the fluid and is based solely on the fluid properties and flow conditions at the surface. Thermal radiation (R_D) and internal heat generation (λ_1) are related to the energy balance of the fluid, but they do not directly influence the fluid flow behavior at the surface. Therefore, they do not affect the skin friction coefficient (C_f).

Carbon nanotubes have enhanced thermal conductivity, which can amplify the transfer of heat between the fluid and the surface. As the solid volume fraction of carbon nanotubes (ϕ)

strengthens, so does the thermal conductivity of the nanofluid, which leads to an advancement in the local Nusselt number (Nu_s). Increment in second-grade fluid parameter (α_1) leads to formation of thicker boundary layer near the solid surface. The thicker boundary layer acts as a barrier to heat transfer, reducing the convective heat transfer coefficient. As a result, the convective heat transfer decreases, resulting in lower local Nusselt number (Nu_s). The Nusselt number (Nu_s) is a dimensionless parameter that relates the convective heat transfer coefficient to the thermal conductivity of the fluid and the characteristic length of the surface. It has been perceived that rate of heat flux raises as an upsurge in radiation parameter (R_D) contains mean absorption coefficient which generates as rise in (R_D). For this reason, the heat transfer rate seems maximizing at every point away from sheet. So the local Nusselt number gets amplified as a rise in radiation parameter (R_D). Moreover an increment in heat generation parameter (λ_1) causes a reduction in local Nusselt number (Nu).

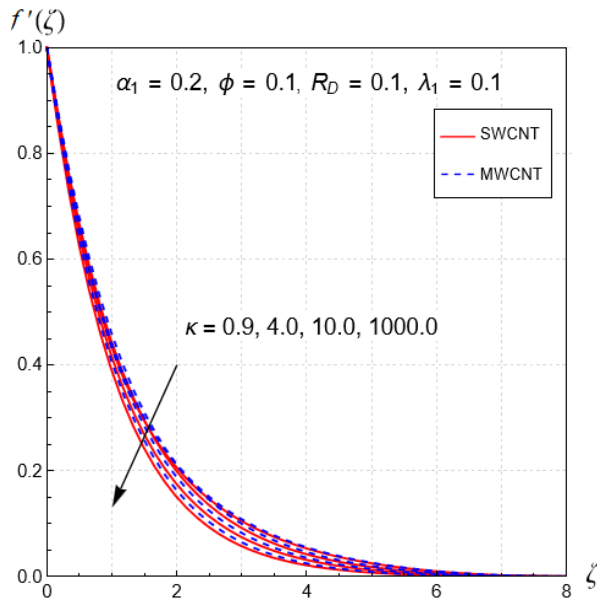


Figure (3.1) Action of (κ) over $f'(\zeta)$

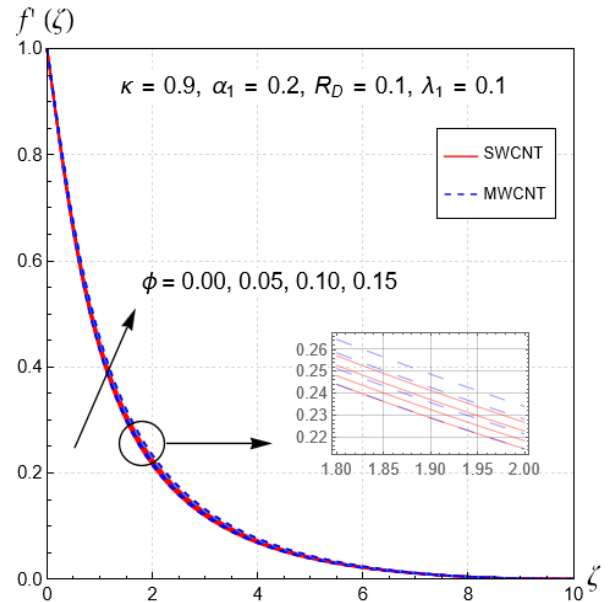


Figure (3.2) Action of (ϕ) over $f'(\zeta)$

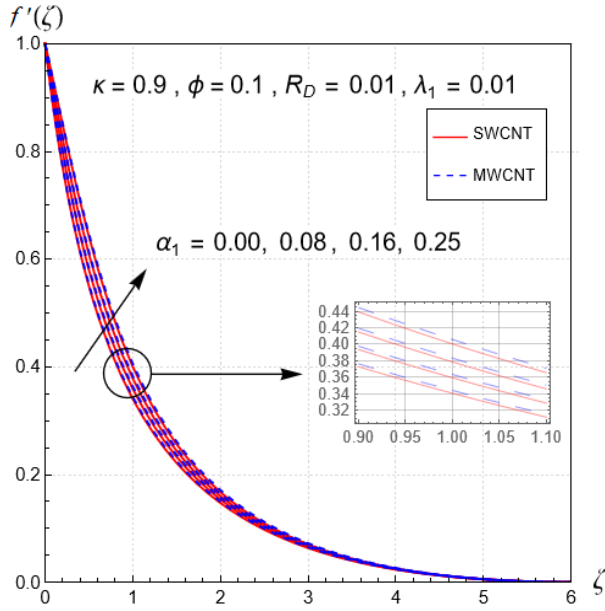


Figure (3.3) Action of (α_1) over $f'(\zeta)$

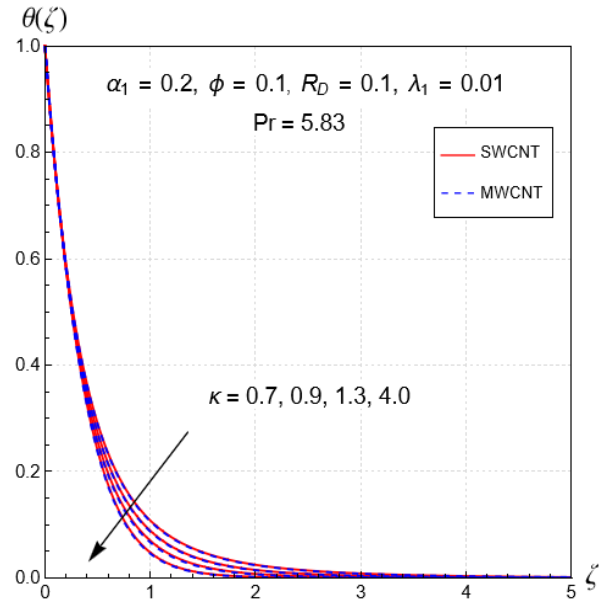


Figure (3.4) Action of (κ) over $\theta(\zeta)$

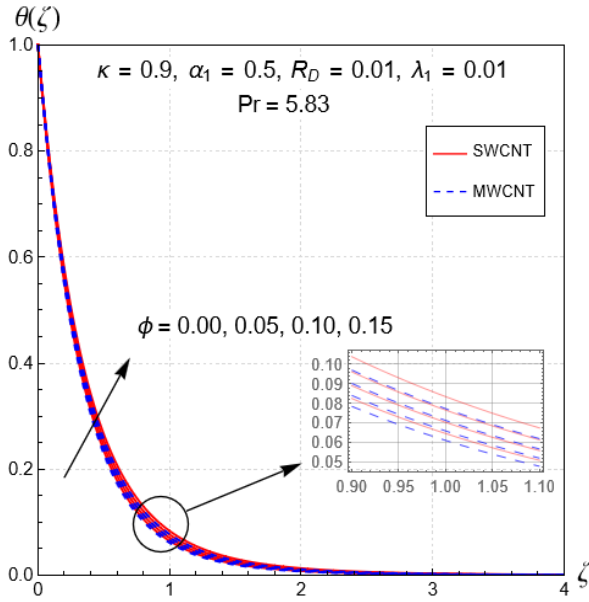


Figure (3.5) Action of (ϕ) over $\theta(\zeta)$

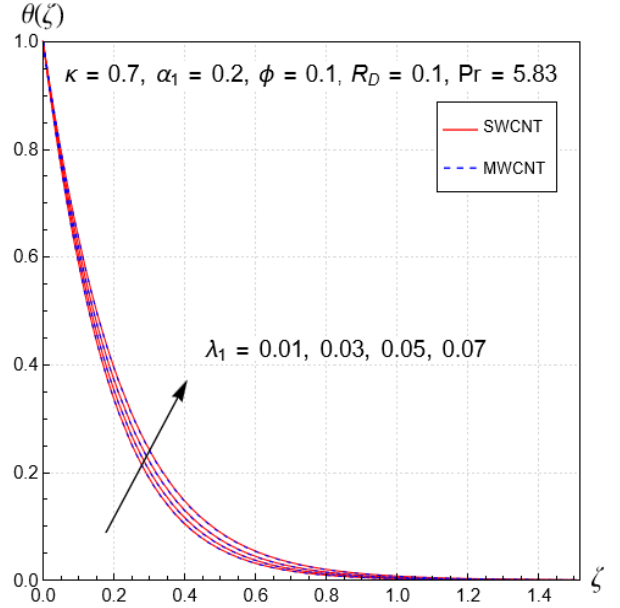


Figure (3.6) Action of (λ_1) over $\theta(\zeta)$

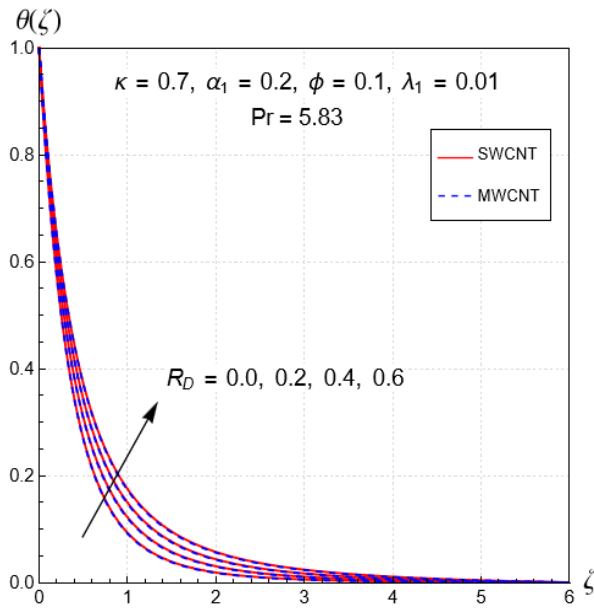


Figure (3.7) Action of (R_D) over $\theta(\zeta)$

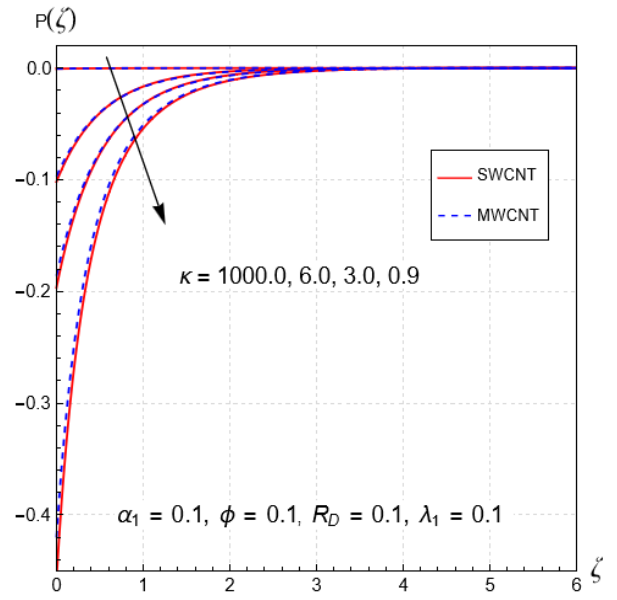


Figure (3.8) Action of (κ) over $P(\zeta)$

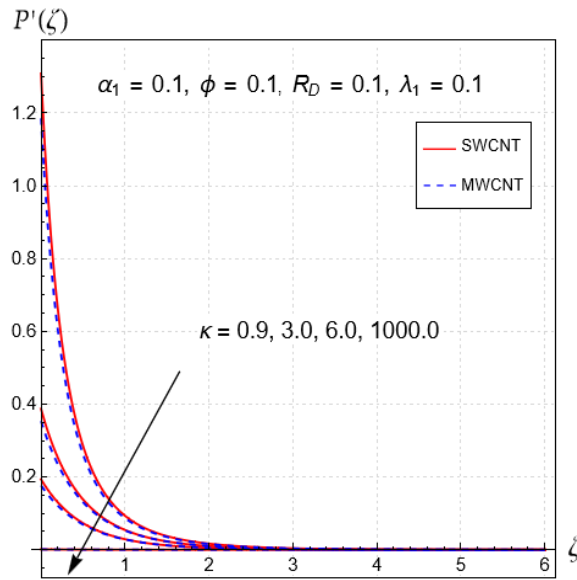


Figure (3.9) Action of (κ) over $P'(\zeta)$

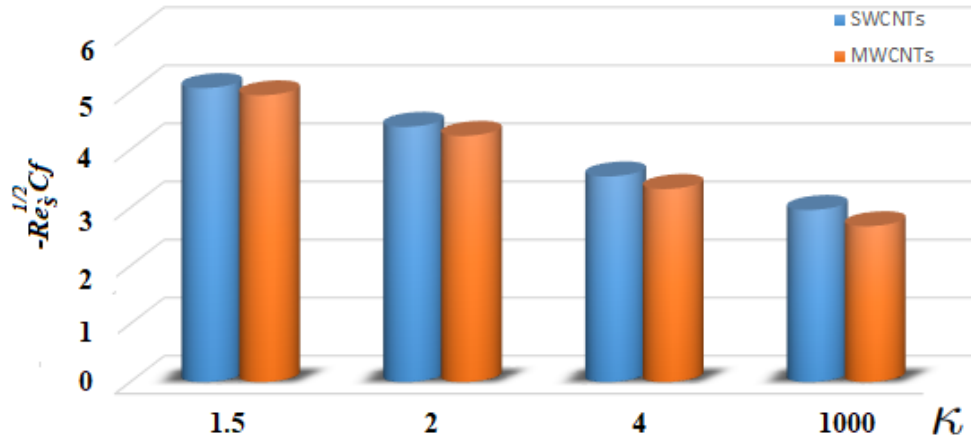


Figure (3.10) Action of (κ) over (Cf)

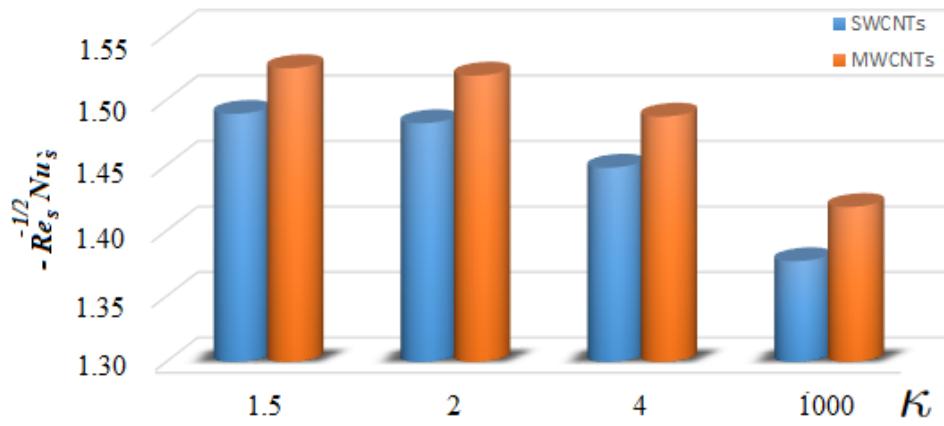


Figure (3.11) Action of (κ) over (Nu)

Table 3.2. Numerical data for local Nusselt number and skin friction coefficient for various parameters.

ϕ	α_1	λ_1	R_D	SWCNTs		MWCNTs	
				$Re_{s_d}^{1/2} C_f$	$Re_{s_d}^{-1/2} Nu_{s_d}$	$Re_{s_d}^{1/2} C_f$	$Re_{s_d}^{-1/2} Nu_{s_d}$
0.0	0.3	0.1	0.1	-3.09927	-1.48942	-3.09927	-1.52424
0.3				-3.56770 ↓	-1.48227 ↑	-3.27669 ↓	-1.51863 ↑
0.5				-3.97289 ↓	-1.44833 ↑	-3.64933 ↓	-1.48731 ↑
0.7				-5.19836	-1.37694	-4.98352	-1.41830
0.1	0.3	0.1	0.1	-3.75080	-1.57626	-3.67442	-1.59220
	0.4			-3.89063 ↓	-1.59300 ↓	-3.80818 ↓	-1.60926 ↓
	0.5			-4.03592 ↓	-1.60758 ↓	-3.94744 ↓	-1.62415 ↓
	0.6			-4.18728	-1.62017	-4.09278	-1.63704
0.1	0.3	0.1	0.1	-3.26908	-1.49443	-3.14391	-1.51198
	0.2			-3.26908 —	-1.39034 ↑	-3.14391 —	-1.41178 ↑
	0.3			-3.26908 —	-1.25988 ↑	-3.14391 —	-1.29045 ↑
	0.4			-3.26908	-1.16865	-3.14391	-1.21177
0.1	0.3	0.1	0.1	-3.26908	-1.49443	-3.14391	-1.51198
		0.3		-3.26908 —	-1.59302 ↓	-3.14391 —	-1.61358 ↓
		0.5		-3.26908 —	-1.68015 ↓	-3.14391 —	-1.70362 ↓
		0.7		-3.26908	-1.75847	-3.14391	-1.78468

Table 3.3. Error analysis of the values of $-\text{Re}_s^{1/2} C_f$ to address the validity of numerical method with $R_D = \lambda_1 = \alpha_1 = 0$.

ϕ	κ	Nagaraja et al. [44]	Current study		Percentage relative absolute difference
			SWCNTs	MWCNTs	
0.0	5	1.15764	1.15763	1.15763	0.000864%
	10	1.07349	1.07349	1.07349	0%
	30	1.02352	1.02353	1.02353	0.000977%
	50	1.01407	1.01405	1.01405	0.001972%

Table 3.4. Comparative analysis of the values of $-\text{Re}_s^{1/2} C_f$ for distinct numerics of κ and ϕ , with $R_D = \lambda_1 = \alpha_1 = 0$.

ϕ	κ	Abbas et al. [43]	Saba et al. [35]		Current study	
			SWCNTs	MWCNTs	SWCNTs	MWCNTs
0.0	5	1.15763	1.15763	1.15763	1.15763	1.15763
	10	1.07349	1.07349	1.07349	1.07349	1.07349
	50	1.01405	1.01405	1.01405	1.01405	1.01405
	1000	1.00079	1.00079	1.00079	1.00079	1.00079
0.1	5	—	1.43781	1.38677	1.43707	1.38669
	10	—	1.32577	1.27251	1.32569	1.27247
	50	—	1.27579	1.22190	1.27549	1.22186

3.3 Conclusions

This investigation scrutinizes heat transmission through a radiative flow of boundary layer nature incorporating heat generation of second grade nanofluid containing carbon nanotubes (SWCNTs and MWCNTs) overtop a curved extending surface. Main highlights are:

- The velocity profile $f'(\zeta)$ gets amplified as an upsurge in solid volume fraction (ϕ) and reduces as an increment in dimensionless curvature (κ).
- The temperature $\theta(\zeta)$ of the fluid rises due to amplification of heat generation parameter (λ_1), radiation parameter (R_D) and solid volume fraction (ϕ) of carbon nanotubes while

an opposite trend is noticed for the upsurge in dimensionless curvature (κ).

- The skin friction coefficient (C_f) drops due to an increment in solid volume fraction (ϕ) and it gets amplified due to a rise in dimensionless curvature (κ) and it remains invariant for upsurge in radiation parameter (R_D) and internal heat generation (λ_1).

- Local Nusselt (Nu_s) number rises as an upsurge in values of solid volume fraction (ϕ), dimensionless curvature (κ) and internal heat generation (λ_1) while it diminishes as a rise in radiation parameter (R_D).

Bibliography

- [1] S.U.S. Choi, Enhancing thermal conductivity of fluids with nanoparticles, *Dev. Appl. Non Newton. Flows.* 232 (1995) 99–105.
- [2] J. Kim, Y.T. Kang, C.K. Choi, Analysis of convective instability and heat transfer characteristics of nanofluids, *Phys. Fluids.* 16 (2004) 2395-2401.
- [3] J. Buongiorno, Convective transport in nanofluids, *J. Heat Transf.* 128 (2006) 240–250.
- [4] R.K. Tiwari, M.K. Das, Heat transfer augmentation in a two-sided lid-driven differentially heated square cavity utilizing nanofluids, *Int. J. Heat Mass Transf.* 50 (2007) 2002-2018.
- [5] W.A. Khan, I. Pop, Boundary-layer flow of a nanofluid past a stretching sheet, *Int. J. Heat Mass Transf.* 53 (2010) 2477–2483.
- [6] A.V. Kuznetsov, D.A. Nield, Natural convective boundary-layer flow of a nanofluid past a vertical plate, *Int. J. Therm. Sci.* 49 (2010) 243–247.
- [7] J. Raza, A.M. Rohmi, Z. Omar, Numerical investigation of copper-water (Cu-Water) nanofluid with different shapes of nanoparticles in a channel with stretching wall: slip effects, *Math. Comput. Appl.* 21 (2016) 43.
- [8] T. Hayat, M. Rashid, A. Alsaedi, MHD convective flow of magnetite-Fe₃O₄ nanoparticles by curved stretching sheet, *Results Phys.* 7 (2017) 3107-3115.
- [9] R.S. Saif, T. Muhammad, H. Sadia, R. Ellahi, Hydromagnetic flow of Jeffrey nanofluid due to a curved stretching surface, *Phys. A: Stat. Mech.* 551 (2020) 0378-4371,

- [10] R.S. Saif, Hashim, M. Zaman, M. Ayaz, Thermally stratified flow of hybrid nanofluids with radiative heat transport and slip mechanism: multiple solutions, *Commun. Theor. Phys.* 74 (2022) 015801.
- [11] J.C. Maxwell, *A Treatise on Electricity and Magnetism*, 3rd ed. Oxford University Press, Oxford, UK, 1904.
- [12] Q.Z. Xue, Model for thermal conductivity of carbon nanotube-based composites, *Phys. B Condens. Matter.* 368 (2005) 302–307.
- [13] U. Khan, N. Ahmed, S.T. Mohyud-Din, Stoke’s first problem for carbon nanotubes suspended nanofluid flow under the effect of slip boundary condition, *J. Nanofluids* 5(2) (2016) 239-244
- [14] T. Hayat , H. Khalid, M. Waqas, A. Alsaedi, Numerical simulation for radiative flow of nanoliquid by rotating disk with carbon nanotubes and partial slip, *Comput. Methods Appl. Mech. Eng.* 341 (2018) 397-408.
- [15] M.I. Khan, F. Shah, T. Hayat, A. Alsaedi, Transportation of CNTs based nanomaterial flow confined between two coaxially rotating disks with entropy generation, *Phys. A: Stat. Mech.* 527 (2019) 121154.
- [16] N. Acharya, R. Bag, P.K. Kundu, On the mixed convective carbon nanotube flow over a convectively heated curved surface, *Heat Transf. Res.* 49 (2020) 1713-1735.
- [17] A.M. Al-Hanaya, F. Sajid, N. Abbas, S. Nadeem, Effect of SWCNT and MWCNT on the flow of micropolar hybrid nanofluid over a curved stretching surface with induced magnetic field, *Sci. Rep.* 10 (2020) 8488.
- [18] S. Ahmad, S. Nadeem, N. Muhammad, M. N. Khan, Cattaneo–Christov heat flux model for stagnation point flow of micropolar nanofluid toward a nonlinear stretching surface with slip effects, *J. Therm. Anal. Calorim.* 143 (2021) 1187–1199.
- [19] M. Ramzan, H. Gul, M.Y. Malik, H.A.S. Ghazwani, Entropy minimization analysis of a partially ionized casson nanofluid flow over a bidirectional stretching sheet with surface catalyzed reaction, *Arab. J. Sci. Eng.* 47 (2022) 15209–15221.
- [20] A. Majeed, A. Zeeshan, T. Alam, Mathematical Analysis of MHD CNT’s of Rotating Nanofluid Flow Over a Permeable Stretching Surface, *Arab. J. Sci. Eng.* 48 (2023) 727–737.

- [21] T. Hayat, M. Sajid, Analytic solution for axisymmetric flow and heat transfer of a second-grade fluid past a stretching sheet, *Int. J. Heat Mass Transf.* 50(1) (2007) 75–84.
- [22] R.S. Saif, T. Hayat, R. Ellahi, T. Muhammad, A. Alsaedi, Stagnation-point flow of second grade nanofluid towards a nonlinear stretching surface with variable thickness, *Results Phys.* 7 (2017) 2821–2830.
- [23] T. Hayat, S. Ahmad, M.I. Khan, A. Alsaedi, Non-Darcy Forchheimer flow of ferromagnetic second-grade fluid, *Results Phys.* 7 (2017) 3419–3424.
- [24] W. Jamshed, K.S. Nisar, R.J.P. Gowda, R.N. Kumar, B.C. Prasannakumara, Radiative heat transfer of second grade nanofluid flow past a porous flat surface: a single-phase mathematical model, *Phys. Scr.* 96(6) (2021) 064006.
- [25] R.J.P. Gowda, H.M. Baskonus, R.N. Kumar, B.C. Prasannakumara, D.G. Prakasha, Computational investigation of Stefan blowing effect on flow of second-grade fluid over a curved stretching sheet, *Int. J. Appl. Comput. Math.* 7(3) (2021) 109.
- [26] S. Pramanik, Casson fluid flow and heat transfer past an exponentially porous stretching surface in presence of thermal radiation, *Ain Shams Eng. J.* 5 (2014) 205–212.
- [27] B.J. Gireesha, B. Mahanthesh, M. M. Rashidi, MHD Boundary Layer Heat and Mass Transfer of a Chemically Reacting Casson Fluid Over a Permeable Stretching Surface with Non-Uniform Heat Source/Sink, *Int. J. Ind. Math.* 7 (2015) 247–260.
- [28] L. Ali, X. Liu, B. Ali, S. Mujeed, S. Abdal, Finite element analysis of thermo-diffusion and multi-slip effects on MHD unsteady flow of Casson nano-fluid over a shrinking/stretching sheet with radiation and heat source, *Appl. Sci.* 9 (2019) 5217.
- [29] M.M. Nandeppanavar, M.C. Kemparaju, N. Raveendra, Double-diffusive free convective flow of Casson fluid due to a moving vertical plate with non-linear thermal radiation, *WJE.* 18(1) (2020) 85–93.
- [30] M.M. Alqarni, M. Bilal, R. Allogmany, E. Tag-Eldin, M.E. Ghoneim, M.F. Yassen, Mathematical analysis of casson fluid flow with energy and mass transfer under the influence of activation energy from a non-coaxially spinning disc, *Front. Energy Res.* 10 (2022) 986284.

- [31] B.C. Sakiadis, Boundary-layer behavior on continuous solid surfaces: II. The boundary layer on a continuous flat surface, *AIChE J.* 7 (1961) 221–225.
- [32] L.J. Crane, Flow past a stretching plate, *J. Appl. Math. Phys. (ZAMP)*. 21 (1970) 645–647.
- [33] M. Sajid, N. Ali, T. Javed, Z. Abbas, Stretching a curved surface in a viscous fluid, *Chin. Phys. Lett.* 27 (2010) 024703.
- [34] T. Hayat, R.S. Saif, R. Ellahi, T. Muhammad, B. Ahmad, Numerical study for Darcy-Forchheimer flow due to a curved stretching surface with Cattaneo-Christov heat flux and homogeneous-heterogeneous reactions, *Results Phys.* 7 (2017) 2886-2892.
- [35] F. Saba, N. Ahmed, S. Hussain, U. Khan, S.T. Mohyud-Din, M. Darus, Thermal Analysis of Nanofluid Flow over a Curved Stretching Surface Suspended by Carbon Nanotubes with Internal Heat Generation, *Appl. Sci.* 8 (2018) 395.
- [36] R. Raza, F. Mabood, R. Naz, S.I. Abdelsalam, Thermal transport of radiative Williamson fluid over stretchable curved surface, *Therm. Sci. Eng. Prog.* 23 (2021) 2451-9049.
- [37] M. Ramzan, A. Dawar, A. Saeed et al., MHD flow of micropolar and Williamson fluids over a bi-directional stretching sheet. *Eur. Phys. J. Plus* 137 (2022) 869.
- [38] A. Majeed, A. Zeeshan, T. Alam, Mathematical Analysis of MHD CNT's of Rotating Nanofluid Flow Over a Permeable Stretching Surface, *Arab. J. Sci. Eng.* 48 (2023) 727–737.
- [39] S. Nasir, A.S. Berrouk, A. Aamir, Z. Shah, Entropy optimization and heat flux analysis of Maxwell nanofluid configured by an exponentially stretching surface with velocity slip, *Sci. Rep.* 13, (2023) 2006.
- [40] S. Sharma, A. Dadheech, A. Parmar, J. Arora, Q. Al-Mdallal, S. Saryana, MHD micro polar fluid flow over a stretching surface with melting and slip effect, *Sci. Rep.* 13 (2023) 10715.
- [41] S. Rosseland, *Astrophysik Und Atom-Theoretische Grundlagen*, Springer: Berlin, Germany, 1931.
- [42] E. Magyari, A. Pantokratoras, Note on the effect of thermal radiation in the linearized Rosseland approximation on the heat transfer characteristics of various boundary layer flows, *Int. Commun. Heat Mass Transf.* 38 (2011) 554–556.

- [43] Z. Abbas, M. Naveed, M. Sajid, Heat transfer analysis for stretching flow over a curved surface with magnetic field, *J. Eng. Thermophys.* 22 (2013) 337–345.
- [44] B. Nagaraja, B.J. Gireesha, Exponential space-dependent heat generation impact on MHD convective flow of Casson fluid over a curved stretching sheet with chemical reaction, *J. Therm. Anal. Calorim.* 143 (2021) 4071–4079.
- [45] H.C. Brinkman, The viscosity of concentrated suspensions and solutions, *J. Chem. Phys.* 20 (1952) 571–581.